On Computing Smooth, Singular, and Nearly Singular Integrals on Implicitly Defined Surfaces

by

Jason R. Wilson

Department of Mathematics
Duke University

Date: _____

Approved:

_____
J. Thomas Beale, Advisor

_____
William K. Allard

_____
Anita T. Layton

_____
John Trangenstein

Dissertation submitted in partial fulfillment of the requirements for the degree of
Doctor of Philosophy in the Department of Mathematics
in the Graduate School of Duke University
2010

Abstract

(Mathematics)

On Computing Smooth, Singular, and Nearly Singular Integrals on Implicitly Defined Surfaces

by

Jason R. Wilson

Department of Mathematics
Duke University

Date: _____

Approved:

_____
J. Thomas Beale, Advisor

_____
William K. Allard

_____
Anita T. Layton

_____
John Trangenstein

An abstract of a dissertation submitted in partial fulfillment of the requirements for the degree of Doctor of Philosophy in the Department of Mathematics in the Graduate School of Duke University
2010

Abstract

We present numerical methods for the approximation of smooth, singular, and nearly singular integrals on implicitly defined surfaces. We begin with a high-order quadrature formula for an integral over a compact smooth implicitly defined hypersurface. Our high-order formula is novel in that it has spectral convergence but does not require a set of overlapping patches. Rather, certain hypersurface points, called quadrature points, must be determined. To find the quadrature points, we search for certain line segments, called brackets, for which the level set function has a sign change at the endpoints. We show that as the segment spacing tends to zero, that each quadrature point must be eventually contained in exactly one bracket. To find the quadrature point within a bracket we use standard one dimensional root finding techniques. Next, we show how to accelerate the process of finding the brackets by restricting the line segment search to cells that are near the hypersurface. Finally, we give an optimal algorithm for finding the quadrature points that has an observed runtime proportional to the number of quadrature points. The high-order convergence of our new quadrature formula is demonstrated numerically on a number of complex implicitly defined surfaces and smooth integrands. Using standard interpolation and finite differencing techniques, we show how to achieve high-order accuracy in the case where the level-set function and integrand are only known at regularly spaced grid points.

We next address the problem of computing double layer and single layer poten-

tials. By using a locally flat cutoff function, we decompose the layer potential into a global part and a local part. We numerically verify that our new quadrature formula has high-order convergence when applied to the global part of a singular double layer potential by computing Gauss's integral on a number of complex implicitly defined surfaces. For the local part, we focus on the single layer potential. In particular, we give a constant runtime complexity algorithm for evaluating the local part of a single layer potential for both the singular and nearly singular cases. To compute the local part, we write the integral in certain local polar coordinates and consider the angular and radial parts separately. We first prove that the angular part can be approximated to high order using the trapezoid rule. In particular, we show that due to our choice of local coordinates, the integrand of the angular part is well approximated by a low degree trigonometric polynomial which is integrated exactly by the trapezoid rule with a small number of quadrature points. We next show that by multiplying the radial integrands by certain helper functions and using a change of variable, the radial integrals can be written in terms of standard integrals that can be precomputed and stored in a lookup table. We demonstrate the high-order convergence of our constant runtime local single layer potential integration method with a number of numerical examples on complex implicitly defined surfaces.

Dedicated to my father, William Wilson (1941-2006)

Contents

List of Tables

List of Figures

Acknowledgements

First, I would like to thank my advisor, Dr. J. Thomas Beale. As a research advisor, Dr. Beale is a paragon. Through all the fits and starts of my nascent research career, he was at my side displaying an enormous amount of support, patience, and guidance. Secondly, I would like to thank my other committee members: Dr. William Allard, Dr. Anita Layton, and Dr. John Trangenstein for their advice, suggestions, and words of encouragement.

Next, I thank my loving wife Teresa who has been a pillar of strength throughout this sometimes difficult and frustrating process. A big thanks to my mother Rose and father Bill who always believed in me and were there to support me when I needed it most. During this journey, I lost my father Bill who was the biggest inspiration in my life. His passion and fire are still with me today and will continue to propel me forward to achieve great things. My newborn son Liam has been a constant source of joy and inspiration as he teaches me about love and life in its purest form. I also want to thank the rest of my family as well as my many wonderful friends for their support and encouragement. Finally, I would like to give a special thanks to Dr. Wayne Aitken whose tireless and passionate instruction at CSU San Marcos made it possible for me to transition from computer science into mathematics.

My research was partially supported by NSF Grant DMS-0806482 and by a Graduate Fellowship at the Statistical and Applied Mathematical Sciences Institute.

1

Introduction

We present numerical methods for the approximation of smooth, singular, and nearly singular integrals on implicitly defined surfaces.

We begin in chapter 2 with a high-order quadrature formula for an integral over a compact smooth implicitly defined hypersurface $\mathcal{S}$. In fact, the convergence rate of our quadrature formula is only limited by the smoothness of the level set function ϕ and the integrand f. This type of convergence is sometimes called *spectral*. More specifically, our method exploits the spectral convergence of the trapezoid rule without the need for the user to generate a set of overlapping coordinate patches and associated partition of unity. Rather than covering $\mathcal{S}$ with overlapping patches, we cover $\mathcal{S}$ with certain overlapping *sets*. For all $1 \leq i \leq d+1$ define the set

$$\mathcal{S}_i = \{x \in \mathcal{S} : |\nu(x) \cdot e_i| > 0\} \tag{1.1}$$

where $\nu(x)$ is the unit normal at x. We show that, assuming the integrand f vanishes outside a compact subset of $\mathcal{S}_i$, the following simple integration formula has spectral convergence

$$\int_{\mathcal{S}} f(y) d\mathcal{S}(y) \approx \sum_{x \in R_{h,i}} \frac{f(x)}{|\nu(x) \cdot e_i|} h^d \tag{1.2}$$

where $R_{h,i}$ is the set of hypersurface points that project to a regular grid with spacing h in the coordinate plane $x_i = 0$. The weights $w(x) = 1/|\nu(x) \cdot e_i|$ correspond to area elements. Note that equation (1.2) allows us to integrate on $\mathcal{S}_i$ as if it were a coordinate patch. We prove the spectral convergence of equation (1.2) in section 2.5.

To handle general integrands f, we introduce a partition of unity to find functions $\{f^i\}_{i=1}^{d+1}$ such that $f(x) = \sum_{i=1}^{d+1} f^i(x)$ for all $x \in \mathcal{S}$ and f^i vanishes outside of a compact set of $\mathcal{S}_i$. Using the unit normal $\nu(x)$, we reduce the problem to finding a partition of unity on the d-sphere, which we denote $\{\psi^{i,\theta}\}_{i=1}^{d+1}$ for some fixed angle $\theta \in (\cos^{-1}(1/\sqrt{d+1}), \pi/2)$. Using the partition of unity and equation (1.2) we arrive at our high-order convergent quadrature formula for general smooth integrands

$$\int_{\mathcal{S}} f(y) d\mathcal{S}(y) \approx \sum_{i=1}^{d+1} \sum_{x \in R_{h,i,\theta}} \frac{\psi^{i,\theta}(\nu(x)) f(x)}{|\nu(x) \cdot e_i|} h^d \tag{1.3}$$

where $R_{h,i,\theta}$ is the set of hypersurface points in $R_{h,i}$ whose unit normal satisfies $|\nu(x) \cdot e_i| > \cos(\theta)$. We call such points *quadrature points*.

The technical difficulty with using equation (1.3) is finding the *quadrature points*. In sections 2.2 and 2.3 we give a simple, provably correct method for finding the quadrature points. In section 2.4, we show how to accelerate the basic quadrature point location algorithm to an observed optimal runtime while maintaining correctness and ease of use. In section 2.6, we give many numerical examples demonstrating the high-order convergence of our new quadrature formula applied to various integrands and surfaces in the case where ϕ, $\nabla\phi$, and f are known exactly. In section 2.7, we demonstrate our methods numerically in the case where knowledge of ϕ and f is restricted to samples on a regular grid. In particular, we give a $O(h^2)$ integration method based on linear interpolation and a $O(h^4)$ integration method based on cubic interpolation. We demonstrate numerically that the expected orders are achieved.

By using a localization method first introduced in [2], a singular or nearly singular

integral can be split into a *global integral* and a *local integral*. More particularly, in chapter 3 we consider the double layer potential with unit density

$$W_0(x) = \int_{\mathcal{S}} \frac{\nu(y) \cdot (x-y)}{|x-y|^3} d\mathcal{S}(y) \tag{1.4}$$

Let $\zeta(r)$ be a smooth, even, and non-negative function with support contained in $[-1,1]$ such that $|\zeta(r)| \leq 1$ and $\zeta(r) = 1$ for $r \in [-\eta, \eta]$ for some $\eta \in (0,1)$. We call ζ a *locally flat* cutoff function. For a given localization radius $\delta > 0$, set $\zeta_\delta(r) = \zeta(r/\delta)$ and define the localized version of $W_0(x)$ as

$$W_0^L(x) = \int_{\mathcal{S}} \frac{\nu(y) \cdot (x-y)}{|x-y|^3} \zeta_\delta(|x-y|) d\mathcal{S}(y)$$

The remainder is called the *global integral* and is defined

$$W_0^G(x) = W_0(x) - W_0^L(x) = \int_{\mathcal{S}} \frac{\nu(y) \cdot (x-y)}{|x-y|^3} (1 - \zeta_\delta(|x-y|)) d\mathcal{S}(y) \tag{1.5}$$

Because of the local flatness of ζ, the global integrand is exactly zero in a ball centered at the evaluation point x with radius $\eta\delta$. Hence, the global integrand is smooth and can be evaluated to high-order using our new high-order quadrature formula. In section 3.1, we demonstrate the high-order convergence of our quadrature formula for evaluation points on several complex implicitly defined surfaces.

In chapter 4, we turn our attention to estimating the *local part* of a single layer potential given by

$$V^L(x) = \int_{\mathcal{S}} \mu(y) \frac{1}{|x-y|} \zeta_\delta(|x-y|) d\mathcal{S}(y) \tag{1.6}$$

As compared to the work in [2, 10], our high-order method for computing the local integral offers the practical benefits of having a constant runtime and handling both singular and nearly singular integrals.

To perform the local integration, we use a local projection onto the tangent plane at x and then write the integral in polar coordinates. We consider the angular integral and the radial integral separately. An overview of how we handle each integral as well as our combined local integration approach is given in section 4.2.

In section 4.3, we prove the surprising fact that the angular integral can be approximated very accurately using the trapezoid rule with only a few angular samples of the radial integral. Our proof technique uses a key aspect of our choice of local coordinates, specifically the projection onto the tangent plane, to show that the radial integral can be well approximated by a low degree trigonometric polynomial which is integrated *exactly* by the trapezoid rule with a small number of quadrature points.

After using the trapezoid rule to approximate the angular integral, we are left with a small number of radial integrals to compute. In sections 4.4 and 4.5, we show that, by multiplying the integrands by certain helper functions and using a change of variable, the radial integrals can be written in terms of standard integrals that can be precomputed and stored in a lookup table. Since the helper functions are chosen to be close to the identity, the remainder terms are small. By keeping track of the remainder terms using a recurrence relation, we develop a high-order integral formula for approximating the radial integrals. The formula depends on derivatives of certain recursively defined functions which are estimated using centered finite difference formulas in section 4.6.

In the final two sections of chapter 4, we present the numerical results for our local integration methods. We consider both singular and nearly singular integrals. In section 4.7, we numerically verify the predicted convergence rates of the angular and radial integration methods in isolation and then together in a combined test. In section 4.8, we numerically verify the accuracy of our constant time local integration method on two complex implicitly defined surfaces with various evaluation points both on and off the surface.

2

High-Order Quadrature On Implicitly Defined Hypersurfaces

2.1 Introduction

Let U be an open subset of $\mathbb{R}^{d+1}$ $(d > 0)$, $\mathcal{S}$ a compact subset of $\mathbb{R}^{d+1}$, and $\phi \in C^{2m+1}(U)$ $(m > 0)$ a real-valued function such that $\nabla\phi$ is nowhere vanishing on $\mathcal{S}$ and

$$\mathcal{S} = \phi^{-1}(0) = \{x \in U : \phi(x) = 0\}$$

Then $\mathcal{S}$ is a compact smooth implicitly defined hypersurface with global defining function ϕ and $C^{2m}(\mathcal{S})$ unit normal

$$\nu(x) = \frac{\nabla\phi(x)}{|\nabla\phi(x)|}$$

In this chapter we develop a high-order quadrature formula for estimating for $f \in C^{2m}(\mathcal{S})$

$$\int_{\mathcal{S}} f(y) d\mathcal{S}(y) \tag{2.1}$$

In fact, the convergence rate of our quadrature formula is only limited by the smoothness of ϕ and f. This type of convergence is sometimes called *spectral*. Our formula

requires little specific knowledge of the surface other than the level set function ϕ and its gradient $\nabla\phi$. See equation (2.9) below for details.

Integration on a smooth compact hypersurface can be reduced to computing integrals over the plane $\mathbb{R}^d$ whose integrands are smooth and vanish outside of a compact set. It is a well known fact that such functions can be integrated to high-order using the d-dimensional trapezoid rule. The reduction to the planar case is accomplished using overlapping coordinate patches and a smooth partition of unity. These ideas lead to a high-order numerical integration method for compact smooth hypersurfaces which we call the *overlapping patch method*. This method has been applied extensively to the computation of singular and nearly singular integrals on surfaces [1, 2, 10]. Other general purpose quadrature methods for surfaces include approximation of delta functions [9] and geometric integration [8]. However, these methods lack the spectral convergence of the overlapping patch method.

By the implicit function theorem and a compactness argument, one can show that by using inverses of coordinate plane projections, a finite set of overlapping patches can always be found that cover a compact smooth implicitly defined hypersurface $\mathcal{S}$. Unfortunately, there is no canonical choice of such overlapping patches. Thus, in most applications of the overlapping patch method to integration, the choice of overlapping patches and associated smooth partition of unity is determined by the user and is surface specific. In [1], for example, spheres and ellipsoids are covered with two stereographic projections. Unfortunately, for complicated implicitly defined surfaces generating a set of overlapping patches and associated partition of unity seems impractical. For problems such as those involving a moving boundary, the level set function will only be known at regularly spaced grid points and maintaining an overlapping patch structure is even more difficult because of the changes in surface geometry as well as the limited amount of available surface information. The manifold work in [11] was a significant step forward in extending the applica-

bility of the overlapping patch approach to high-order quadrature on complicated surfaces. However, the approach seems limited to static surfaces that are designed using a set of user supplied control points. Because of these practical limitations, the overlapping patch method is not useful as a general purpose numerical integration method for compact smooth implicitly defined hypersurfaces despite the high-order convergence rate.

Our new numerical integration method has the high-order convergence rate of the overlapping patch method but lacks the practical limitations. More specifically, our method exploits the spectral convergence of the trapezoid rule without the need for the user to generate a set of overlapping coordinate patches and associated partition of unity. Rather than covering $\mathcal{S}$ with overlapping patches, we cover $\mathcal{S}$ with certain overlapping *sets*. For all $1 \leq i \leq d+1$ define the set

$$\mathcal{S}_i = \{x \in \mathcal{S} : |\nu(x) \cdot e_i| > 0\} \tag{2.2}$$

where $\{e_i\}_{i=0}^{d+1}$ is a standard basis for $\mathbb{R}^{d+1}$. Note that $\mathcal{S}_i$ contains all points in $\mathcal{S}$ that are not orthogonal to e_i. A key component of our integration method is a high-order convergent, patch independent quadrature formula, see equation (2.6), for estimating integrals with integrands that vanish outside of a compact subset of $\mathcal{S}_i$.

To handle general integrands f, we introduce a partition of unity to find functions $\{f^i\}_{i=1}^{d+1}$ such that $f(x) = \sum_{i=1}^{d+1} f^i(x)$ for all $x \in \mathcal{S}$ and f^i vanishes outside of a compact set of $\mathcal{S}_i$. We first design a universal partition of unity on the unit d-sphere, $S^d = \{u \in \mathbb{R}^{d+1} : |u| = 1\}$. We start with the smooth bump function defined as $b(r) = e^{(r^2)/(r^2-1)}$ for $|r| < 1$ and $b(r) = 0$ otherwise. See figure A.1 in appendix A for a graph. Next we choose a fixed angle $\theta \in (\cos^{-1}(1/\sqrt{d+1}), \pi/2)$ and for each

$1 \leq i \leq d+1$ and $u \in S^d$ we define

$$\omega^i(u) = \cos^{-1}(|u \cdot e_i|), \qquad \psi^{i,\theta}(u) = \frac{b(\omega^i(u)/\theta)}{\sum_{j=1}^{d+1} b(\omega^j(u)/\theta)} \tag{2.3}$$

Because $\theta > \cos^{-1}(1/\sqrt{d+1})$, the functions $\psi^{i,\theta}$ are well-defined and furthermore

1. For all $1 \leq i \leq d+1$, we have that $\psi^{i,\theta} \in C^\infty(S^d)$.
2. For all $u \in S^d$, we have that $\sum_{i=1}^{d+1} \psi^{i,\theta}(u) = 1$
3. For all $1 \leq i \leq d+1$, the function $\psi^{i,\theta}$ vanishes outside the compact subset of S_i^d given by
$$\{u \in S^d : |u \cdot e_i| \geq \cos(\theta)\}$$

To make use of the above partition of unity for a general surface $\mathcal{S}$ we use the smooth unit normal $\nu(x) \in C^{2m}(\mathcal{S})$. More specifically, we note that the functions $\{\psi^{i,\theta} \circ \nu\}_{i=1}^{d+1}$ satisfy

1. For all $1 \leq i \leq d+1$, we have that $\psi^{i,\theta} \circ \nu \in C^{2m}(\mathcal{S})$.
2. For all $x \in \mathcal{S}$, we have that $\sum_{i=1}^{d+1} \psi^{i,\theta}(\nu(x)) = 1$
3. For all $1 \leq i \leq d+1$, the function $\psi^{i,\theta} \circ \nu$ vanishes outside the compact subset of $\mathcal{S}_i$ given by
$$\{x \in \mathcal{S} : |\nu(x) \cdot e_i| \geq \cos(\theta)\} \tag{2.4}$$

Thus, we have the formula

$$\int_{\mathcal{S}} f(y) d\mathcal{S}(y) = \sum_{i=1}^{d+1} \int_{\mathcal{S}} \psi^{i,\theta}(\nu(y)) f(y) d\mathcal{S}(y) \tag{2.5}$$

where the integrands $f^i(y) = \psi^{i,\theta}(\nu(y)) f(y)$ vanish outside a compact subset of $\mathcal{S}_i$.

The formula given by equation (2.5) allows us to reduce integration on $\mathcal{S}$ to integration on compact subsets of $\mathcal{S}_i$. The following lemma gives a high-order convergent formula for such integrals. We defer the proof until section 2.5.

Lemma 1. *Let $\mathcal{S} \subseteq \mathbb{R}^{d+1}$ be a compact smooth implicitly defined hypersurface with global defining function $\phi \in C^{2m+1}(U)$. Let $\nu \in C^{2m}(\mathcal{S})$ be the associated smooth unit normal and let $f \in C^{2m}(\mathcal{S})$ be given. Assume that f vanishes outside of a compact set K and that $K \subseteq \mathcal{S}_i$ for some $1 \leq i \leq d+1$. Then there exists a $C > 0$ such that for all $h > 0$ we have*

$$\left| \int_{\mathcal{S}} f(y) d\mathcal{S}(y) - \sum_{x \in R_{h,i}} \frac{f(x)}{|\nu(x) \cdot e_i|} h^d \right| \leq C h^{2m} \tag{2.6}$$

where

$$R_{h,i} = \{x \in \mathcal{S} : p^i(x) \in h\mathbb{Z}^d\} \tag{2.7}$$

and $p^i : \mathbb{R}^{d+1} \to \mathbb{R}^d$ is the projection function defined by

$$p^i(x) = (x_1, \ldots, x_{i-1}, x_{i+1}, \ldots, x_{d+1}) \tag{2.8}$$

The basic idea of the proof is that since K is compact and does not include points whose normal direction is orthogonal to e_i, we can cover K with a finite number of overlapping open sets that can be smoothly projected onto a coordinate plane $x_i = 0$. We use the inverses of these projections as coordinate patches as well as a smooth partition of unity to write the surface integral as a sum of integrals over $\mathbb{R}^d$ with compactly supported integrands. Fortunately, our trapezoid rule approximation turns out to be independent of the choice of coordinate patches and partition of unity. Finally, the weights $w(x) = 1/|\nu(x) \cdot e_i|$ correspond to the inverse projection area elements.

By combining equations (2.5) and (2.6) we arrive at our main quadrature result which is given in the next theorem.

Theorem 2. *Let $\mathcal{S} \subseteq \mathbb{R}^{d+1}$ be a compact smooth implicitly defined hypersurface with global defining function $\phi \in C^{2m+1}(U)$. Let $\nu \in C^{2m}(\mathcal{S})$ be the associated smooth unit normal and let $f \in C^{2m}(\mathcal{S})$ be given. Then there exists a $C > 0$ such that for all $h > 0$ we have*

$$\left| \int_{\mathcal{S}} f(y) d\mathcal{S}(y) - \sum_{i=1}^{d+1} \sum_{x \in R_{h,i,\theta}} \frac{\psi^{i,\theta}(\nu(x)) f(x)}{|\nu(x) \cdot e_i|} h^d \right| \leq C h^{2m} \tag{2.9}$$

where

$$R_{h,i,\theta} = \{x \in R_{h,i} : |\nu(x) \cdot e_i| > \cos(\theta)\} \tag{2.10}$$

The technical difficulty with using equation (2.9) is finding the sets $\{R_{h,i,\theta}\}_{i=1}^{d+1}$ which we call the *quadrature points*. Since the quadrature points lie along regularly spaced *grid lines*, finding them is a problem similar to implicit ray casting. However, because quadrature points are well separated, finding the quadrature points is simpler than finding all of the hypersurface intersection points. In section 2.2 we give a simple algorithm for finding the quadrature points and give a correctness proof in section 2.3. In section 2.4, we show how to accelerate the basic quadrature point location algorithm to an observed optimal runtime while maintaining correctness and ease of use. In section 2.5, we prove a more general form of lemma 1 and theorem 2.

In the final two sections, we present numerical results for certain smooth integrands. In section 2.6, we focus on the case where ϕ, $\nabla\phi$, and f are known exactly. In particular, we give many examples demonstrating the high-order convergence of our new quadrature formula applied to various integrands and surfaces. In section 2.7, we assume that the knowledge of ϕ and f is restricted to samples on a regular grid. In particular, no knowledge of $\nabla\phi$ is assumed. We show that by using interpolation and finite difference formulas, the exact quadrature formula sum can be approximated resulting in a small *approximation error*. The overall integration error is shown to be the sum of the quadrature error, which is the difference between the

integral and the exact sum, and the approximation error. We show through numerical example that by using linear interpolation and second order finite differences, the approximation error is $O(h^2)$ and by using cubic interpolation and fourth order finite differences, the approximation error is $O(h^4)$.

2.2 Finding the Quadrature Points

Assume that $\mathcal{S}$ is a compact smooth implicitly defined hypersurface with global defining function $\phi \in C^2(U)$, and define the set $D = \{1, \ldots, d+1\}$. For some given quadrature spacing $h > 0$ and cutoff angle $\theta \in (\cos^{-1}(1/\sqrt{d+1}), \pi/2)$, we consider the problem of finding the quadrature points $\{R_{h,i,\theta}\}_{i=1}^{d+1}$ defined by equations (2.10) and (2.7). The quadrature points lie along regularly spaced grid lines. These grid lines are images of the map L with domain $\mathbb{Z}^d \times D$ given by

$$L(\lambda, i) = \{x \in \mathbb{R}^{d+1} : p^i(x) = \lambda h\}$$

where $p^i(x)$ is the projection function defined by equation (2.8).

The first step in finding the quadrature points is to cut these grid lines into segments of length $H > 0$ where H is called the *segment spacing*. More specifically, the segments are images of the map S with domain $\mathbb{Z}^d \times D \times \mathbb{Z}$ given by

$$S(\lambda, i, j) = \{x \in L(\lambda, i) : x \cdot e_i \in [jH, (j+1)H]\} \tag{2.11}$$

The endpoints of these segments are particularly important. We define the two endpoint functions $A : \mathbb{Z}^d \times D \times \mathbb{Z} \to \mathbb{R}^{d+1}$ and $B : \mathbb{Z}^d \times D \times \mathbb{Z} \to \mathbb{R}^{d+1}$ by

$$A(\lambda, i, j) = \iota^i(\lambda h) + jHe_i$$

$$B(\lambda, i, j) = \iota^i(\lambda h) + (j+1)He_i$$

where the embedding functions $\{\iota^i\}_{i=1}^{d+1} : \mathbb{R}^d \to \mathbb{R}^{d+1}$ are defined by

$$\iota^i(\alpha) = (\alpha_1, \ldots, \alpha_{i-1}, 0, \alpha_{i+1}, \ldots, \alpha_d)$$

We define the *sign* function s by $s(r) = 1$ for $r \geq 0$ and $s(r) = -1$ otherwise. Note that unlike some other sign functions given in the literature, s is never zero. The sign function s is helpful in dealing with the special case in which a quadrature point is an endpoint.

A segment $S(\lambda, i, j)$ is called a *bracket* if

$$s(\phi(A(\lambda, i, j)))s(\phi(B(\lambda, i, j))) < 0 \tag{2.12}$$

The brackets are important because provided that the segment spacing H is chosen small enough, relative to certain derivative bounds on ϕ, the brackets are the only segments that can contain quadrature points. We will also show that for sufficiently small H, if a quadrature point is an endpoint of some bracket, then equation (2.12) combined with the definition of s ensures that the adjacent segment sharing the endpoint is not also a bracket. The task of locating the brackets is called *bracketing*.

2.2.1 A Simple Bracketing Algorithm

In this section we give a simple bracketing algorithm that only requires ϕ on a regular grid with spacing $h > 0$ where h is the quadrature spacing. For some integer $k \geq 0$, define the segment spacing to be $H = 2^k h$. Since $\mathcal{S}$ is compact, it is bounded. Let $b \in \mathbb{R}^{d+1}$ specify a bounding box for $\mathcal{S}$. More specifically, define $M = \{x \in \mathbb{R}^{d+1} : |x|_\infty \leq b\}$ and suppose $\mathcal{S} \subseteq M$.

Our simple bracketing algorithm is as follows. For each triple (λ, i, j) such that the segment $S(\lambda, i, j) \cap M \neq \varnothing$, check equation (2.12). If it is true, then $S(\lambda, i, j)$ is a bracket.

For each grid line $L(\lambda, i)$ that intersects the bounding box M, the algorithm checks $O(1/H)$ segments. Since there are $O(1/h^d)$ grid lines that intersect M, the algorithm checks a total of $O(1/(h^d H))$ segments.

If H is a constant then the algorithm checks $O(1/h^d)$ segments which is optimal

because there are $O(1/h^d)$ brackets. However, finding the right value of H to guarantee correctness of the bracketing algorithm requires knowledge of certain derivative bounds and so is not practical in all situations. If we choose H so that $H = O(h)$, the algorithm requires $O(1/h^{d+1})$ steps which is considerably worse than optimal. However, the advantage is that since $H \to 0$ as $h \to 0$, the segment spacing H will eventually be small enough to guarantee correctness of the bracketing algorithm. An alternative that shares some of the advantages of each of the extreme approaches is to choose H so that $H = O(h^p)$ for some $p \in (0, 1)$. In section 2.4, we show how to accelerate this basic bracketing algorithm by using a simple cell covering method.

2.2.2 Checking The Brackets For Quadrature Points

A segment $S(\lambda, i, j)$ that is a bracket always contains at least one hypersurface point because by equation (2.12) and the definition of s we have that

$$\phi(A(\lambda, i, j)))\phi(B(\lambda, i, j))) \leq 0 \tag{2.13}$$

We will show that provided H is chosen small enough, if a quadrature point is in a bracket then there are no other hypersurface points in that same bracket (see part 3 of corollary 5). Thus, it suffices to find a single hypersurface point in each bracket and test that point to see if it is a quadrature point. If it is not, then the bracket cannot contain a quadrature point.

Since $S(\lambda, i, j)$ is a line segment, finding a hypersurface point can be reduced to finding a root of a one-dimensional equation. More specifically, given the triple (λ, i, j) we define $f(t) = \phi(\iota^i(\lambda h) + tjHe_i)$ and look for a $\tau \in [0, 1]$ such that $f(\tau) = 0$. Because of equation (2.13), it is always possible to find a root $\tau \in [0, 1]$ using the bisection method. Since the bisection method only has linear convergence, we improve the performance by using a simple adaptive procedure. First, we try to find a root with Newton's method using the midpoint of the bracket as an initial guess.

If Newton's method fails to converge after some number of iterations, we switch to the bisection method which is guaranteed to converge. In practice, Newton's method converges to a root very quickly for all but a small number of brackets.

2.3 The Separation Lemma and Its Consequences

Assume that $\mathcal{S}$ is a compact smooth implicitly defined hypersurface with global defining function $\phi \in C^2(U)$. In section 2.2, we gave a simple procedure for finding the quadrature points $\{R_{h,i,\theta}\}_{i=1}^{d+1}$ and claimed that the method works provided that the segment spacing $H > 0$ is chosen small enough relative to certain derivative bounds on ϕ. In this section, we give the theory that justifies this claim.

2.3.1 Derivative Bounds

Since $\mathcal{S}$ is compact and $\nabla\phi$ is nonvanishing on $\mathcal{S}$, $|\nabla\phi|$ is bounded from below on $\mathcal{S}$ by

$$C_1 = \min_{x\in\mathcal{S}} |\nabla\phi(x)| > 0 \tag{2.14}$$

For a matrix $A : \mathbb{R}^{d+1} \to \mathbb{R}^{d+1}$ we set

$$\|A\| = \max_{|u|=1} |Au|$$

For $x \in \mathbb{R}^{d+1}$, define the sets

$$B(x,r) = \{y \in \mathbb{R}^{d+1} : |x-y| < r\}, \quad \overline{B}(x,r) = \{y \in \mathbb{R}^{d+1} : |x-y| \le r\}$$

Since $\mathcal{S}$ is compact and U is open, we can choose $\delta > 0$ such that the compact set

$$K_\delta = \bigcup_{x\in\mathcal{S}} \overline{B}(x,\delta) \tag{2.15}$$

satisfies $K_\delta \subseteq U$. For $x \in U$, let $\nabla^2\phi(x)$ denote the Hessian matrix of ϕ at x and set

$$C_2 = \max_{x\in K_\delta} \|\nabla^2\phi(x)\| \tag{2.16}$$

We will ultimately show that the method of section 2.2 finds all of the quadrature points provided that the segment spacing H satisfies

$$H \leq \min(2\cos(\theta)C_1/C_2, \delta) \tag{2.17}$$

Our proof technique is to show that for sufficiently small H, the quadrature points are *well separated*. We formalize this idea in the next section.

2.3.2 The Separation Lemma

A ray in $\mathbb{R}^{d+1}$ can be represented parametrically as $r(t) = x + tu$ where $x \in \mathbb{R}^{d+1}$ and u is a unit vector. For a given ray $r(t)$ we define

$$f(t) = \phi(r(t)), \qquad g(t) = \nabla\phi(r(t)), \qquad n(t) = \frac{f'(t)}{|g(t)|} \tag{2.18}$$

The derivatives of f and g are

$$f'(t) = \nabla\phi(r(t)) \cdot u = g(t) \cdot u, \qquad g'(t) = \nabla^2\phi(r(t))u \tag{2.19}$$

In the following lemma we show that $f''(t)$ is uniformly bounded for points $r(t)$ near the surface.

Lemma 3. *Suppose that $f(\tau) = 0$. Then for all $t \in [-\delta + \tau, \delta + \tau]$ we have*

$$|f''(t)| \leq C_2$$

Proof. Let $t \in [-\delta + \tau, \delta + \tau]$. Since $|t - \tau| \leq \delta$ we have that $|(r(t) - r(\tau)| \leq \delta$ and hence $r(t) \in K_\delta$ where K_δ is given in equation (2.15). Thus by equation (2.16), we have $\|\nabla^2\phi(r(t))\| \leq C_2$. By considering equation (2.19), using the Cauchy-Schwarz inequality, and properties of the matrix norm we compute

$$|f''(t)| = |\left(\nabla^2\phi(r(t))u\right) \cdot u| \leq \|\nabla^2\phi(r(t))\| \leq C_2$$

□

Next we state and prove the critical separation lemma.

Lemma 4. *Let $\theta \in (0, \pi/2)$. Suppose that $H \leq \min(2\cos(\theta)C_1/C_2, \delta)$ and that*

$$f(\tau) = 0, \qquad |n(\tau)| > \cos(\theta) \tag{2.20}$$

Then for all $t_1 \in [\tau - H, \tau)$ and all $t_2 \in (\tau, \tau + H]$ we have that $f(t_1)f(t_2) < 0$.

Proof. Let $t_1 \in [\tau - H, \tau)$ and $t_2 \in (\tau, \tau + H]$ be given. By Taylor's theorem and the fact that $f(\tau) = 0$, we have

$$f(t_1) = f'(\tau)(t_1-\tau)+\frac{f''(t^*)}{2}(t_1-\tau)^2, \quad f(t_2) = f'(\tau)(t_2-\tau)+\frac{f''(t^{**})}{2}(t_2-\tau)^2 \tag{2.21}$$

where $t^* \in (t_1, \tau)$ and $t^{**} \in (\tau, t_2)$. By lemma 3 and the assumptions we have that

$$\left|\frac{f''(t^*)}{2}|t_1 - \tau|^2\right| \leq \frac{C_2}{2}H|t_1 - \tau| \leq \frac{C_2}{2}(2\cos(\theta)C_1/C_2)|t_1 - \tau| = \cos(\theta)C_1|t_1 - \tau|$$

and similarly

$$\left|\frac{f''(t^{**})}{2}|t_2 - \tau|^2\right| \leq \frac{C_2}{2}H|t_2 - \tau| \leq \frac{C_2}{2}(2\cos(\theta)C_1/C_2)|t_2 - \tau| = \cos(\theta)C_1|t_2 - \tau|$$

Since $|n(\tau)| > \cos(\theta)$ and $|g(\tau)| \geq C_1$ we have $|f'(\tau)| > C_1\cos(\theta)$ and thus

$$|f'(\tau)(t_1 - \tau)| > C_1\cos(\theta)|t_1 - \tau| \geq \left|\frac{f''(t^*)}{2}|t_1 - \tau|^2\right| \tag{2.22}$$

and similarly

$$|f'(\tau)(t_2 - \tau)| > C_1\cos(\theta)|t_2 - \tau| \geq \left|\frac{f''(t^{**})}{2}|t_2 - \tau|^2\right| \tag{2.23}$$

Since $|n(\tau)| > \cos(\theta) > 0$ we have that $|f'(\tau)| > 0$. If $f'(\tau) > 0$ we have $f(t_1) < 0$ by equations (2.22) and (2.21) and $f(t_2) > 0$ by equations (2.23) and (2.21). Similarly, If $f'(\tau) < 0$ we have $f(t_1) > 0$ and $f(t_2) < 0$. □

2.3.3 Applications to Finding Quadrature Points

Let $\mathcal{S}$ be given and define δ, C_1, and C_2 as in section 2.3.1. The first two parts of the following corollary deal with ensuring the correctness of our bracketing algorithm. The third part handles our method for finding quadrature points within brackets. More specifically, assume that H satisfies equation (2.24). Then the first two parts of the corollary imply that each quadrature point is in *exactly* one bracket. The third part gives us the fact that if a bracket contains a quadrature point, then the quadrature point is the *only* hypersurface point in the bracket.

Corollary 5. *Suppose that*

$$H \leq \min(2\cos(\theta)C_1/C_2, \delta) \tag{2.24}$$

and $x \in R_{h,i,\theta}$ *for some* $i \in D$. *Let* $p^i(x) = h\lambda$ *for some* $\lambda \in \mathbb{Z}^d$.

1. *If* $x \cdot e_i \in (jH, (j+1)H)$ *for some* $j \in \mathbb{Z}$, *then*

$$s(\phi(A(\lambda, i, j)))s(\phi(B(\lambda, i, j))) < 0$$

2. *If* $x \cdot e_i = jH$ *for some* $j \in \mathbb{Z}$, *then one of*

$$s(\phi(A(\lambda, i, j)))s(\phi(B(\lambda, i, j))) < 0$$

   or

$$s(\phi(A(\lambda, i, j-1)))s(\phi(B(\lambda, i, j-1))) < 0$$

   is true but not both.

3. *Suppose* $S(\lambda, i, j)$ *is a bracket containing the quadrature point* x. *If* $\phi(y) = 0$ *and* $y \in S(\lambda, i, j)$, *then* $y = x$.

Proof. Let $r(t) = \iota^i(h\lambda) + te_i$ and define f, g, and n as in equation (2.18). Let $\tau = x \cdot e_i$. Since $x \in R_{h,i,\theta}$ we have that $\phi(x) = 0$ and thus $f(\tau) = 0$. Furthermore, we have $|\nu(x) \cdot e_i| > \cos(\theta)$ and thus

$$|n(\tau)| = \frac{|f'(\tau)|}{|g(\tau)|} = \frac{|g(\tau) \cdot e_i|}{|g(\tau)|} = \frac{|\nabla\phi(x) \cdot e_i|}{|\nabla\phi(x)|} = |\nu(x) \cdot e_i| > \cos(\theta)$$

Thus the conditions of equation (2.20) hold and by lemma 4 we have for all $t_1 \in [\tau - H, \tau)$ and all $t_2 \in (\tau, \tau + H]$ that $f(t_1)f(t_2) < 0$. For the first part of the corollary assume that $\tau = x \cdot e_i \in (jH, (j+1)H)$. Then since $jH \in [\tau - H, \tau)$ and $(j+1)H \in (\tau, \tau + H]$ we have that $f(jH)f((j+1)H) < 0$. Thus

$$\phi(A(\lambda, i, j))\phi(B(\lambda, i, j)) = \phi(\iota^i(h\lambda) + jHe_i)\phi(\iota^i(h\lambda) + (j+1)He_i)$$

$$= f(jH)f((j+1)H) < 0$$

and since $\phi(A(\lambda, i, j)) \neq 0$ and $\phi(B(\lambda, i, j)) \neq 0$ we have

$$s(\phi(A(\lambda, i, j)))s(\phi(B(\lambda, i, j))) < 0$$

as well. The second part of the corollary follows from lemma 4 as well because if $f(jH) = 0$ then $f((j-1)H)f((j+1)H) < 0$. The third part follows because according to lemma 4, if $f(\tau) = 0$ and $|n(\tau)| > \cos(\theta)$, then f is nonzero on the set $[\tau - H, \tau) \cup (\tau, \tau + H]$. □

2.4 Cell Covering and Fast Bracketing

Assume that $\mathcal{S}$ is a compact smooth implicitly defined hypersurface with global defining function $\phi \in C^2(U)$. Let $h > 0$ be the quadrature spacing and $H = 2^k h$ be the segment spacing. Assume throughout that $k \geq 1$ and that ϕ and $\nabla\phi$ are known on a regular grid with spacing h. In this section, we use the additional knowledge

of $\nabla\phi$ at the grid points to accelerate the bracketing algorithm described in section 2.2.1. Our *fast bracketing* algorithm is guaranteed to work provided that

$$H \leq \min(2\cos(\theta)C_1/C_2, 2\delta/\sqrt{d+1}) \tag{2.25}$$

Note that if $d \leq 3$, then if H satisfies equation (2.17), then H also satisfies (2.25).

The basic idea of our fast bracketing algorithm is that by grouping the segments into cells, we can use a cell covering algorithm to significantly reduce the number of segments that need to be checked for brackets. Our cell covering algorithm is based on the simple proximity test given in the next section.

2.4.1 The Proximity Lemma

Suppose that $y \in \mathbb{R}^{d+1}$ and a point $x \in \mathcal{S}$ is nearby. In this section, we determine how the information $\phi(y)$ and $\nabla\phi(y)$ can be used to detect the proximity of the hypersurface point $x \in \mathcal{S}$. Let δ, C_1, and C_2 be defined as in section 2.3.1. The following lemma gives our proximity test.

Lemma 6. *Suppose that for some $\epsilon > 0$ and $\alpha \in (0,1)$ we have that*

$$\epsilon \leq \min(\alpha C_1/C_2, \delta) \tag{2.26}$$

Further suppose that $x \in \mathcal{S}$, $y \in \mathbb{R}^{d+1}$, and $|x-y| \leq \epsilon$. Then we have that

$$|\phi(y)| \leq \left(1 + \frac{\alpha}{2(1-\alpha)}\right)|\nabla\phi(y)|\epsilon \tag{2.27}$$

Proof. If $x = y$, then $\phi(y) = 0$ and equation (2.27) is trivially true. Thus we can assume that $x \neq y$. Let $u = (x-y)/|x-y|$ and $\tau = |x-y|$. Note that $x = y + \tau u$, $|\tau| \leq \epsilon$ and $|u| = 1$. Set $f(t) = \phi(y+tu)$ and note that $f(0) = \phi(y)$ and $f(\tau) = \phi(x) = 0$. By Taylor's theorem we have that

$$f(\tau) = f(0) + f'(0)\tau + f''(t^*)\tau^2/2 \tag{2.28}$$

where t^* is between 0 and τ. Since $|t^* - \tau| \leq \epsilon \leq \delta$ we see that $f''(t^*) \leq C_2$ by lemma 3. Using the fact that $f(\tau) = 0$ and applying the triangle inequality to equation (2.28) we have

$$|f(0)| \leq |f'(0)||\tau| + C_2|\tau|^2/2$$

Since $f(0) = \phi(y)$ and $f'(0) = \nabla\phi(y) \cdot u$ we have that

$$|\phi(y)| \leq |\nabla\phi(y) \cdot u||\tau| + C_2|\tau|^2/2$$

Since $|\tau| \leq \epsilon$ we have by equation (2.26) that $C_2|\tau| \leq C_2\epsilon \leq \alpha C_1$. Using this fact as well as the Cauchy-Schwarz inequality we see that

$$|\phi(y)| \leq |\nabla\phi(y)|\epsilon + \alpha C_1\epsilon/2 \tag{2.29}$$

Next, we relate C_1 and $|\nabla\phi(y)|$. Since $x \in \mathcal{S}$, we have by equation (2.14) that

$$|\nabla\phi(x)| \geq C_1 \tag{2.30}$$

Combining the mean value inequality, equation (2.16), and equation (2.26) we get

$$|\nabla\phi(x) - \nabla\phi(y)| \leq C_2|x - y| \leq C_2\epsilon \leq \alpha C_1 \tag{2.31}$$

Using the triangle inequality and equations (2.30) and (2.31) we see that

$$|\nabla\phi(y)| \geq |\nabla\phi(x)| - |\nabla\phi(x) - \nabla\phi(y)| \geq C_1 - \alpha C_1 = (1 - \alpha)C_1 \tag{2.32}$$

Finally, we combine equations (2.29) and (2.32) to deduce equation (2.27). □

2.4.2 Cell Covering I : Problem Statement and Theory

Our principal application of the proximity lemma given in section 2.4.1 is to the problem of cell covering. Let $H > 0$ be a parameter called the *cell width*. For our application of cell covering to fast bracketing, the cell width will always be equal to

the segment spacing. The space $\mathbb{R}^{d+1}$ is the union of *cells* that are images of the map C with domain $\mathbb{Z}^{d+1}$ given by

$$C(\sigma) = \{x \in \mathbb{R}^{d+1} : (x - \sigma H) \in [0, H]^{d+1}\} \tag{2.33}$$

The problem of *cell covering* is to determine an index set $I \subseteq \mathbb{Z}^{d+1}$ such that

1. If $\sigma \in \mathbb{Z}^{d+1}$ and $C(\sigma) \cap \mathcal{S} \neq \varnothing$ then $\sigma \in I$.

2. $|I| = O(1/H^d)$

The first requirement ensures that our chosen set of cells cover the hypersurface $\mathcal{S}$. The second requirement ensures that our cell covers are *efficient*. Since there are $O(1/H^d)$ cells that intersect $\mathcal{S}$, our second requirement is optimal. In this section we give a solution to the cell covering problem and prove that it satisfies the first requirement for sufficiently small cell widths H. With a computational example, we demonstrate that the second requirement is also satisfied. We leave the analysis of the efficiency of our method as future work.

The following corollary of lemma 6 provides a necessary condition for a cell $C(\sigma)$ to intersect the hypersurface $\mathcal{S}$. We define the cell center point map $P : \mathbb{Z}^{d+1} \to \mathbb{R}^{d+1}$

$$P(\sigma) = \sigma H + 1_{d+1} H/2 \tag{2.34}$$

where $1_{d+1} \in \mathbb{Z}^{d+1}$ is the integer vector with all components equal to 1.

Corollary 7. *Let $H > 0$ be the cell width and $\alpha \in (0, 1)$. Assume that*

$$H \leq \min(2(\alpha/\sqrt{d+1})C_1/C_2, 2\delta/\sqrt{d+1}) \tag{2.35}$$

If $C(\sigma) \cap \mathcal{S} \neq \varnothing$, then

$$|\phi(P(\sigma))| \leq \left(1 + \frac{\alpha}{2(1-\alpha)}\right) |\nabla\phi(P(\sigma))|(H/2)\sqrt{d+1} \tag{2.36}$$

Proof. Let $x \in C(\sigma) \cap \mathcal{S}$ and set $y = P(\sigma)$. Then by equations (2.33) and (2.34) we have $|x - y| \leq \epsilon$ where $\epsilon = (H/2)\sqrt{d+1}$. Since $\epsilon \leq \delta$ and $\epsilon \leq \alpha(C_1/C_2)$ by equation (2.35), all of the conditions of lemma 6 are satisfied and hence

$$|\phi(y)| \leq \left(1 + \frac{\alpha}{2(1-\alpha)}\right) |\nabla\phi(y)|\epsilon = \left(1 + \frac{\alpha}{2(1-\alpha)}\right) |\nabla\phi(y)|(H/2)\sqrt{d+1} \quad (2.37)$$

□

2.4.3 Cell Covering II : Algorithm and Efficiency Test

In this section, we give our simple cell covering algorithm which is based on equation (2.36). We then give some numerical evidence that demonstrates the efficiency of our method on an implicitly defined surface. Let $b \in \mathbb{R}^{d+1}$ specify a bounding box for $\mathcal{S}$. More specifically, define $M = \{x \in \mathbb{R}^{d+1} : |x|_\infty \leq b\}$ and suppose $\mathcal{S} \subseteq M$.

Our simple cell covering algorithm is as follows. Pick $H > 0$ and $\alpha \in (0, 1)$. For each $\sigma \in \mathbb{Z}^{d+1}$ such that $C(\sigma) \cap M \neq \varnothing$ check equation (2.36). If the result is true, then add σ to the cell cover index set I.

For each cell $C(\sigma)$ that intersects the bounding box M, the algorithm does $O(1)$ steps. Since there are $O(1/H^{d+1})$ cells that intersect M, the algorithm requires $O(1/H^{d+1})$ total steps. Provided that H and α satisfy equation (2.35), corollary 7 guarantees that the algorithm finds all cells that intersect $\mathcal{S}$.

We test the efficiency of our cell covering method numerically using an implicitly defined surface. More specifically, we compute cell covers of the torus given as the zero set of

$$\phi(x) = (x_1^2 + x_2^2 + x_3^2 + R^2 - r^2)^2 - 4R^2(x_1^2 + x_2^2) \quad (2.38)$$

with specific parameters $R = 3$ and $r = 1$. We use $\alpha = 2/3$ throughout. Given our choice of parameters, equation (2.36) simplifies to

$$|\phi(P(\sigma))| \leq |\nabla\phi(P(\sigma))|H\sqrt{3}$$

The results for various values of H are shown in table 2.1. Recall that $|I|$ is the number of cells in the cover. Since the order in table 2.1 is converging to 2, we

Table 2.1: Cell Covering Efficiency

$-(\log_2 H)$	$\lvert I\rvert$	order
3	25872	
4	102976	1.99
5	414104	2.01
6	1662080	2.00

deduce that $|I| = O(1/H^2)$. Since $d = 2$, the order is optimal. Thus, this numerical test suggests that our cell covering algorithm is efficient and that $|I| = O(1/H^d)$ in general.

2.4.4 Fast Bracketing

Let $h > 0$ be the quadrature spacing and $H = 2^k h$ for some $k \geq 1$. Assume that H is the segment spacing and the cell width. We say that a segment $S(\lambda, i, j)$, see equation (2.11), is *covered* by the cell $C(\sigma)$ if

$$\sigma \cdot e_i = j \tag{2.39}$$

and

$$(\lambda - p^i(\sigma)2^k) \in \mathbb{Z}^d \cap [0, 2^k)^d \tag{2.40}$$

Note that each segment is covered by *exactly* one cell. More specifically, the segment $S(\lambda, i, j)$ is only covered by the cell $C(\iota^i(\lfloor \lambda/2^k \rfloor) + je_i)$. Also note that there are $(d+1)2^{kd} = (d+1)(H/h)^d$ segments covered by each cell.

Our fast bracketing algorithm is as follows.

1. Use the cell covering algorithm given in section 2.4.3 with $\alpha = \cos(\theta)\sqrt{d+1}$ to find a cell cover index set I.

2. For each $\sigma \in I$ check the segments covered by $C(\sigma)$ for brackets.

We use $\alpha = \cos(\theta)\sqrt{d+1}$ to get the requirement on H given by equation (2.35) to match the requirement on H given by equation (2.25). Note that since $\theta \in (\cos^{-1}(1/\sqrt{d+1}), \pi/2)$, we have that $\alpha \in (0,1)$ as required. As discussed in section 2.4.3, the cell covering step of the fast bracketing algorithm requires $O(1/H^{d+1})$ steps. Furthermore, for each $\sigma \in I$ there are $O((H/h)^d)$ segments to check. Assuming that our cell covering algorithm is efficient, we have that $|I| = O(1/H^d)$. Thus, our fast bracketing algorithm has a runtime complexity of

$$O(1/H^{d+1}) + O(1/h^d) \tag{2.41}$$

2.4.5 Optimal Runtime and Guaranteed Correctness

To balance the runtime complexity of the two steps of the fast bracketing algorithm shown in equation (2.41), we choose H such that

$$H = O\left(h^{\frac{d}{d+1}}\right) \tag{2.42}$$

Using this choice of H, the runtime complexity of the fast bracketing algorithm becomes the optimal $O(1/h^d)$. In practice we set

$$k = \left\lceil \log_2\left(h^{\frac{d}{d+1}}/h\right)\right\rceil \tag{2.43}$$

and note that $k \geq 1$ and $H = 2^k h$ satisfies equation (2.42).

The important advantage of the balanced version of the fast bracketing method is that it has the optimal runtime complexity without requiring a fixed segment spacing H. Because $H \to 0$ as $h \to 0$ by equation (2.42), the segment spacing H will eventually be small enough to satisfy equation (2.25). Thus, the balanced version of the fast bracketing method has the combined advantages of an optimal runtime as well as guaranteed correctness as $h \to 0$. Furthermore, the algorithm does not require knowledge of any derivative bounds on ϕ.

2.5 Quadrature Formula Proofs

In this section, we prove lemma 1 and theorem 2 in a slightly more general form; see lemma 9 and theorem 10 below. In particular, we relax the requirements that $\mathcal{S}$ be compact and implicitly defined.

We begin with the definition of a general hypersurface [4]. A subset $\mathcal{S}$ of $\mathbb{R}^{d+1}$ $(d > 0)$ is called a hypersurface of class C^k $(1 \leq k \leq \infty)$ if for every $x \in \mathcal{S}$ there is an open set $V \subseteq \mathbb{R}^{d+1}$ containing x and a real-valued function $\phi \in C^k(V)$ such that $\nabla\phi$ is nowhere vanishing on $\mathcal{S} \cap V$ and

$$\mathcal{S} \cap V = \{y \in V : \phi(x) = 0\}$$

We call ϕ a *local defining function* for $\mathcal{S}$ near x.

Our results make a critical use of a well known quadrature fact that follows immediately from the multivariate Euler-Maclaurin formula (for a proof see [3]).

Lemma 8. *For $d > 0$ and $m > 0$, let $f \in C^{2m}(\mathbb{R}^d)$. Suppose that f vanishes outside of a compact set $K \subseteq \mathbb{R}^d$. Then there exists a $C > 0$ such that for all $h > 0$*

$$\left| \int_{\mathbb{R}^d} f(y)dy - \sum_{\sigma \in \mathbb{Z}^d \cap K} f(\sigma h)h^d \right| \leq Ch^{2m} \tag{2.44}$$

The following lemma generalizes lemma 1. The definition of $\mathcal{S}_i$ is given in equation (2.2).

Lemma 9. *Let $\mathcal{S} \subseteq \mathbb{R}^{d+1}$ $(d > 0)$ be a hypersurface of class C^{2m+1} $(m > 0)$ with unit normal $\nu \in C^{2m}(\mathcal{S})$. Let $f \in C^{2m}(\mathcal{S})$ and suppose that f vanishes outside of compact set K and that $K \subseteq \mathcal{S}_i$ for some $1 \leq i \leq d+1$. Then there exists a C such that for all $h > 0$*

$$\left| \int_{\mathcal{S}} f(y)d\mathcal{S}(y) - \sum_{x \in R_{h,i} \cap K} \frac{f(x)}{|\nu(x) \cdot e_i|} h^d \right| \leq Ch^{2m} \tag{2.45}$$

where $R_{h,i}$ is defined by equation (2.7).

Proof. Let $y \in K$ and $\phi : V \to \mathbb{R}$ be a local defining function for $\mathcal{S}$ near y. By assumption we know that $|\nu(y) \cdot e_i| > 0$ and thus $|\nabla\phi(y) \cdot e_i| > 0$. By the implicit function theorem, there exists an open set $V_y \subseteq V$, with $y \in V_y$, an open set $W_y \subseteq \mathbb{R}^d$, with $p^i(y) \in W_y$, and a C^{2m+1} mapping $\Phi^y : W_y \to \mathcal{S}$ such that $\Phi^y(p^i(z)) = z$ for all $z \in V_y \cap \mathcal{S}$. Since K is compact, we can choose a finite set $\{y^1, \ldots, y^N\}$ such that $\{V_{y^j}\}_1^N$ is an open cover of K. Choose a smooth partition of unity $\{\Psi^j\}_1^N : \mathcal{S} \to \mathbb{R}$ on K subordinate to the covering $\{V_{y^j}\}_1^N$. For brevity we set $\Phi^j = \Phi^{y_j}$. Using the partition of unity as well as the coordinate functions we write

$$\int_{\mathcal{S}} f(y) d\mathcal{S}(y) = \sum_{j=1}^{N} \int_{\mathbb{R}^d} \frac{\Psi^j(\Phi^j(\alpha)) f(\Phi^j(\alpha))}{|\nu(\Phi^j(\alpha)) \cdot e_i|} d\alpha$$

with the understanding that the integrand is zero for α outside $\mathrm{supp}(\Psi^j \circ \Phi^j)$. Equation (2.44) implies that for each $1 \leq j \leq N$ there exists a C_j such that for all $h > 0$

$$\left| \int_{\mathbb{R}^d} \frac{\Psi^j(\Phi^j(\alpha)) f(\Phi^j(\alpha))}{|\nu(\Phi^j(\alpha)) \cdot e_i|} d\alpha - \sum_{\sigma \in \mathbb{Z}^d} \frac{\Psi^j(\Phi^j(\sigma h)) f(\Phi^j(\sigma h))}{|\nu(\Phi^j(\sigma h)) \cdot e_i|} h^d \right| \leq C_j h^{2m}$$

since the integrand is in $C^{2m}(\mathbb{R}^d)$ and has compact support. Next, we have the identity

$$\sum_{j=1}^{N} \sum_{\sigma \in \mathbb{Z}^d} \frac{\Psi^j(\Phi^j(\sigma h)) f(\Phi^j(\sigma h))}{|\nu(\Phi^j(\sigma h)) \cdot e_i|} h^d = \sum_{j=1}^{N} \sum_{x \in R_{h,i} \cap K} \frac{\Psi^j(x) f(x)}{|\nu(x) \cdot e_i|} h^d$$

where we used the fact that $\mathrm{supp}(f) \subseteq K$. Switching the summation order and using the fact that $\sum_{j=1}^{N} \Psi^j(x) = 1$ for all $x \in K$, we see that

$$\sum_{j=1}^{N} \sum_{x \in R_{h,i} \cap K} \frac{\Psi^j(x) f(x)}{|\nu(x) \cdot e_i|} h^d = \sum_{x \in R_{h,i} \cap K} \sum_{j=1}^{N} \frac{\Psi^j(x) f(x)}{|\nu(x) \cdot e_i|} h^d = \sum_{x \in R_{h,i} \cap K} \frac{f(x)}{|\nu(x) \cdot e_i|} h^d$$

Thus the result follows for $C = \sum_{j=1}^{N} C_j$ by the triangle inequality. □

Next we prove a more general version of theorem 2.

Theorem 10. *Let $\mathcal{S} \subseteq \mathbb{R}^{d+1}$ $(d > 0)$ be a hypersurface of class C^{2m+1} $(m > 0)$ with unit normal $\nu \in C^{2m}(\mathcal{S})$. Let $f \in C^{2m}(\mathcal{S})$ and suppose that f vanishes outside of compact set $K \subseteq \mathcal{S}$. Then there exists a $C > 0$ such that for all $h > 0$ we have*

$$\left| \int_{\mathcal{S}} f(y) d\mathcal{S}(y) - \sum_{i=1}^{d+1} \sum_{x \in R_{h,i,\theta} \cap K} \frac{\psi^{i,\theta}(\nu(x)) f(x)}{|\nu(x) \cdot e_i|} h^d \right| \leq C h^{2m} \tag{2.46}$$

where $\psi^{i,\theta}$ is defined in equation (2.3) and $R_{h,i,\theta}$ is defined in equation (2.10).

Proof. Since the proof is similar to the one of theorem 2 outlined in section 2.1, we focus on the differences. Since $\mathcal{S}$ is not necessarily compact, we have that for all $1 \leq i \leq d+1$, the function $\psi^{i,\theta} \circ \nu$ vanishes outside of the *closed* subset of $\mathcal{S}_i$ given by equation (2.4). However, the integrands $f^i(y) = \psi^{i,\theta}(\nu(y)) f(y)$ still vanish outside of a compact subset of $\mathcal{S}_i$ because $\text{supp}(f^i)$ is a closed subset of the compact set K and hence is also compact. Thus the result follows by combining equations (2.5) and (2.45). □

2.6 Numerical Results I : Exact Level Set Functions

In this section we assume that ϕ, $\nabla\phi$, and f are known exactly. In this case, we can can compute the trapezoid rule sum in equation (2.9) exactly. Thus, the only source of error is the *quadrature error*. For bracketing, we use the balanced fast bracketing method described in section 2.4.5. We start by computing some surface areas.

2.6.1 Surface Area

Although our primary focus will be the surface case ($d = 2$), the theory developed in this chapter applies to any hypersurface dimension. We illustrate the generality

of our quadrature method by computing the surface area of the 3-sphere which we know to be $2\pi^2$. For this test we use $\theta = 68°$. The results are shown in table 2.2.

Table 2.2: Surface Area : 3-Sphere

$-(\log_2 h)$	rel err	order
4	$5.29 \cdot 10^{-5}$	
5	$3.17 \cdot 10^{-7}$	7.38
6	$1.60 \cdot 10^{-9}$	7.63
7	$5.15 \cdot 10^{-13}$	11.60

Next, we compute the surface area of the torus which we defined in equation (2.38). The exact surface area is $12\pi^2$. For this test we use $\theta = 63°$. The results are shown in table 2.3.

Table 2.3: Surface Area : Torus

$-(\log_2 h)$	rel err	order
4	$1.99 \cdot 10^{-5}$	
5	$9.65 \cdot 10^{-7}$	4.37
6	$7.31 \cdot 10^{-9}$	7.04
7	$8.41 \cdot 10^{-12}$	9.76
8	$1.68 \cdot 10^{-16}$	15.61

Next, consider the prolate ellipsoid given as the zero set of the function

$$\phi(x) = x_1^2/a^2 + x_2^2 + x_3^2 - 1 \tag{2.47}$$

We compute the surface area for $a = 5$ and $a = 10$ using $\theta = 62.5°$. The results are shown in table 2.4. As indicated by the numerical results, as a becomes large, the surface area is more difficult to compute accurately because of the large derivatives at the ellipsoid tip.

Table 2.4: Surface Area : Prolate Ellipsoids

$-(\log_2 h)$	a	rel err	order	a	rel err	order
6	5	$1.36 \cdot 10^{-7}$		10	$8.70 \cdot 10^{-7}$	
7	5	$2.60 \cdot 10^{-9}$	5.70	10	$1.83 \cdot 10^{-8}$	5.57
8	5	$1.32 \cdot 10^{-11}$	7.63	10	$3.08 \cdot 10^{-10}$	5.89
9	5	$1.40 \cdot 10^{-14}$	9.88	10	$1.02 \cdot 10^{-12}$	8.23

2.6.2 Verifying the Gauss-Bonnet Theorem

In this section, we use our quadrature formula to integrate the Gaussian curvature over the three surfaces given in appendix B and verify the Gauss-Bonnet theorem. Similar integration tests appear in [8].

For a closed surface $\mathcal{S}$, the Gauss-Bonnet theorem tells us that

$$\int_{\mathcal{S}} \kappa_1 \kappa_2 d\mathcal{S} = 4\pi(1-g) \tag{2.48}$$

where g is the genus of the surface and $\kappa_1\kappa_2$ is the Gaussian curvature. A formula for the Gaussian curvature in terms of ϕ, $\nabla\phi$, and $\nabla^2\phi$ appears in [8]. For our numerical tests, we use this formula to compute the Gaussian curvature at a quadrature point exactly. We use analytic formulas for ϕ, $\nabla\phi$ and $\nabla^2\phi$.

For the double torus, we expect the value of the integral in equation (2.48) to be -4π because $g = 2$. The numerical results are given in table 2.5. We use $\theta = 62.5°$.

Table 2.5: Verifying Gauss-Bonnet : Double Torus

$-(\log_2 h)$	rel err	order
7	$1.95 \cdot 10^{-4}$	
8	$1.31 \cdot 10^{-5}$	3.89
9	$4.67 \cdot 10^{-7}$	4.82
10	$3.92 \cdot 10^{-9}$	6.89
11	$5.86 \cdot 10^{-12}$	9.39
12	$5.44 \cdot 10^{-16}$	13.40

For the orthocircles surface, we expect the value of the integral in equation (2.48) to be -24π because $g = 7$. The numerical results are given in table 2.6. We use $\theta = 62.5°$.

Table 2.6: Verifying Gauss-Bonnet : Orthocircles

$-(\log_2 h)$	rel err	order
6	$5.56 \cdot 10^{-3}$	
7	$4.04 \cdot 10^{-4}$	3.78
8	$1.46 \cdot 10^{-5}$	4.79
9	$9.36 \cdot 10^{-8}$	7.29
10	$3.53 \cdot 10^{-10}$	8.05
11	$1.57 \cdot 10^{-13}$	11.14

For the tanglecube surface, we expect the value of the integral in equation (2.48) to be -16π because $g = 5$. The numerical results are given in table 2.7. We use $\theta = 63.5°$.

Table 2.7: Verifying Gauss-Bonnet : Tanglecube

$-(\log_2 h)$	rel err	order
5	$5.37 \cdot 10^{-5}$	
6	$1.73 \cdot 10^{-6}$	4.96
7	$4.62 \cdot 10^{-8}$	5.23
8	$1.77 \cdot 10^{-10}$	8.03
9	$4.12 \cdot 10^{-14}$	12.07

2.7 Numerical Results II : Sampled Level Set Functions

In this section we assume that the knowledge of ϕ and f is restricted to samples on a regular grid. In particular, no knowledge of $\nabla\phi$ is assumed. We first recall the trapezoid rule sum part of our high-order quadrature formula given in equation (2.9)

$$\sum = \sum_{i=1}^{d+1} \sum_{x \in R_{h,i,\theta}} \frac{\psi^{i,\theta}(\nu(x)) f(x)}{|\nu(x) \cdot e_i|} h^d$$

Given our limited knowledge of ϕ and f, we will have to approximate the quadrature point x, the unit normal function ν, and the integrand f. We put bars over these three quantities and call the resulting sum the *approximate* trapezoid rule sum.

$$\overline{\sum} = \sum_{i=1}^{d+1} \sum_{\bar{x} \in R_{h,i,\theta}} \frac{\psi^{i,\theta}(\bar{\nu}(\bar{x}))\bar{f}(\bar{x})}{|\bar{\nu}(\bar{x}) \cdot e_i|} h^d$$

We call the difference $|\Sigma - \overline{\Sigma}|$ the *approximation error* and the difference $|\int - \Sigma|$ the *quadrature error* where $\int$ is the exact value of the integral. To estimate the *overall error* we use the triangle inequality as follows.

$$\left| \int - \overline{\sum} \right| \leq \left| \int - \sum \right| + \left| \sum - \overline{\sum} \right|$$

Thus, the overall error is bounded by the sum of the quadrature error and the approximation error.

We give two methods for approximating the trapezoid rule sum. We call the first method the *linear* method and the second method the *cubic* method. We will see in the numerical results section that the approximation error of the linear method is $O(h^2)$ and the approximation error of the cubic method is $O(h^4)$. In the linear method for approximating the trapezoid rule sum, we use linear interpolation and second order finite differences as detailed in the following algorithm.

1. Find the brackets using the simple bracketing algorithm described in section 2.2.1.

2. Refine each bracket of width H to a bracket of width h using bisection.

3. For each refined bracket, compute $\bar{x}$ using linear interpolation and compute $\bar{\nu}$ at the endpoints of the bracket using second order finite differences of ϕ.

4. For each $\bar{x}$, compute $\bar{\nu}(\bar{x})$ and $\bar{f}(\bar{x})$ using linear interpolation.

In the cubic method for approximating the trapezoid rule sum, we use cubic interpolation and fourth order finite differences as detailed in the following algorithm.

1. Find the refined brackets as in the linear method.

2. For each refined bracket, form a cubic interpolant of ϕ by using the ϕ values at the endpoints of the two adjacent segments. Set $\bar{x}$ to a root of the cubic interpolant inside the refined bracket. Compute $\bar{\nu}$ at the endpoints of the two adjacent segments using fourth order finite differences of ϕ.

3. For each $\bar{x}$, compute $\bar{\nu}(\bar{x})$ and $\bar{f}(\bar{x})$ using cubic interpolation.

2.7.1 Surface Area

First we describe some of the information contained in the following tables. The *quad err* column contains the relative errors $|\int - \Sigma|/|\int|$. The *approx err* column contains the relative errors $|\Sigma - \overline{\Sigma}|/|\Sigma|$. Finally, the *total err* column contains the relative errors $|\int - \overline{\Sigma}|/|\int|$.

For our first test case we consider computing the surface area of the torus as in section (2.6.1). We use $\theta = 63°$. In table 2.8, we show the results obtained by using the linear method. In table 2.9, we show the results obtained by using the cubic method. The tables show that the linear method has a $O(h^2)$ approximation error

Table 2.8: Surface Area of a Torus : Linear Method

$-(\log_2 h)$	quad err	order	approx err	order	total err	order
4	$1.99 \cdot 10^{-5}$		$3.20 \cdot 10^{-4}$		$3.00 \cdot 10^{-4}$	
5	$9.65 \cdot 10^{-7}$	4.37	$7.66 \cdot 10^{-5}$	2.06	$7.75 \cdot 10^{-5}$	1.95
6	$7.31 \cdot 10^{-9}$	7.04	$1.96 \cdot 10^{-5}$	1.97	$1.96 \cdot 10^{-5}$	1.99
7	$8.41 \cdot 10^{-12}$	9.76	$4.89 \cdot 10^{-6}$	2.00	$4.89 \cdot 10^{-6}$	2.00
8	$1.68 \cdot 10^{-16}$	15.61	$1.22 \cdot 10^{-6}$	2.01	$1.22 \cdot 10^{-6}$	2.01

and the cubic method has a $O(h^4)$ approximation error. Note also that in the case of

Table 2.9: Surface Area of a Torus : Cubic Method

$-(\log_2 h)$	quad err	order	approx err	order	total err	order
4	$1.99 \cdot 10^{-5}$		$7.53 \cdot 10^{-8}$		$2.00 \cdot 10^{-5}$	
5	$9.65 \cdot 10^{-7}$	4.37	$4.40 \cdot 10^{-9}$	4.10	$9.61 \cdot 10^{-7}$	4.38
6	$7.31 \cdot 10^{-9}$	7.04	$2.87 \cdot 10^{-10}$	3.94	$7.03 \cdot 10^{-9}$	7.10
7	$8.41 \cdot 10^{-12}$	9.76	$1.79 \cdot 10^{-11}$	4.00	$9.54 \cdot 10^{-12}$	9.52
8	$1.68 \cdot 10^{-16}$	15.61	$1.11 \cdot 10^{-12}$	4.01	$1.11 \cdot 10^{-12}$	3.10

the linear method the approximation error is the dominant error while in the case of the cubic method the quadrature error is the dominant error until h gets very small. This suggests that using a higher order approximation method may not have much benefit for practical problems.

2.7.2 Verifying the Gauss-Bonnet Theorem

For our second test case we consider verifying the Gauss-Bonnet theorem for the tanglecube surface as in section 2.6.2. We use $\theta = 63.5°$. In this case, the integrand is interpolated to get values off of the grid. In table 2.10, we show the results obtained by using the linear method. In table 2.11, we show the results obtained by using the cubic method. If the quadrature error and approximation error are roughly the same size but of different sign, fortuitous cancellation occurs which can obscure the nature of the convergence. This is illustrated clearly in the last column of table 2.11. However, by considering the two errors separately, we see that the convergence rates are indeed as expected.

Table 2.10: Gauss-Bonnet for Tanglecube : Linear Method

$-(\log_2 h)$	quad err	order	approx err	order	total err	order
5	$5.37 \cdot 10^{-5}$		$7.22 \cdot 10^{-4}$		$7.75 \cdot 10^{-4}$	
6	$1.73 \cdot 10^{-6}$	4.96	$1.79 \cdot 10^{-4}$	2.01	$1.77 \cdot 10^{-4}$	2.13
7	$4.62 \cdot 10^{-8}$	5.23	$4.57 \cdot 10^{-5}$	1.97	$4.57 \cdot 10^{-5}$	1.96
8	$1.77 \cdot 10^{-10}$	8.03	$1.11 \cdot 10^{-5}$	2.04	$1.11 \cdot 10^{-5}$	2.04
9	$4.12 \cdot 10^{-14}$	12.07	$2.80 \cdot 10^{-6}$	1.99	$2.80 \cdot 10^{-6}$	1.99

Table 2.11: Gauss-Bonnet for Tanglecube : Cubic Method

$-(\log_2 h)$	quad err	order	approx err	order	total err	order
5	$5.37 \cdot 10^{-5}$		$1.02 \cdot 10^{-5}$		$6.39 \cdot 10^{-5}$	
6	$1.73 \cdot 10^{-6}$	4.96	$6.81 \cdot 10^{-7}$	3.91	$1.05 \cdot 10^{-6}$	5.93
7	$4.62 \cdot 10^{-8}$	5.23	$4.27 \cdot 10^{-8}$	3.99	$3.46 \cdot 10^{-9}$	8.24
8	$1.77 \cdot 10^{-10}$	8.03	$2.77 \cdot 10^{-9}$	3.95	$2.95 \cdot 10^{-9}$	0.23
9	$4.12 \cdot 10^{-14}$	12.07	$1.73 \cdot 10^{-10}$	4.00	$1.73 \cdot 10^{-10}$	4.09

3

Double Layer Potentials and Gauss's Integral

In this chapter we consider the problem of computing the global part of a double layer potential with unit density for evaluations points on the surface using our high-order quadrature formula given in equation (2.9).

For an evaluation point $x \in \mathbb{R}^3$, we write a double layer potential as

$$W(x) = \int_{\mathcal{S}} \mu(y) \frac{\partial}{\partial \nu(y)} \frac{1}{|x-y|} d\mathcal{S}(y)$$

where $\mu : \mathcal{S} \to \mathbb{R}$ is called the density. Calculating the normal derivative gives

$$\frac{\partial}{\partial \nu(y)} \frac{1}{|x-y|} = \frac{\nu(y) \cdot (x-y)}{|x-y|^3}$$

Thus

$$W(x) = \int_{\mathcal{S}} \mu(y) \frac{\nu(y) \cdot (x-y)}{|x-y|^3} d\mathcal{S}(y)$$

The double layer potential with unit density

$$W_0(x) = \int_{\mathcal{S}} \frac{\nu(y) \cdot (x-y)}{|x-y|^3} d\mathcal{S}(y) \tag{3.1}$$

is sometimes called Gauss's Integral [7]. The exact value is given by

$$W_0(x) = \begin{cases} -4\pi, & \text{for } x \text{ inside } \mathcal{S} \\ 0, & \text{for } x \text{ outside } \mathcal{S} \\ -2\pi, & \text{for } x \in \mathcal{S} \end{cases}$$

If $x \in S$, the above integrals are weakly singular. A straightforward application of the trapezoid rule to overlapping surface patches is only $O(h)$ accurate where h is the quadrature spacing. For the double layer potential, the order of the singularity can be reduced be using the formula

$$W(x) = \int_{\mathcal{S}} (\mu(y) - \mu(x)) \frac{\nu(y) \cdot (x - y)}{|x - y|^3} d\mathcal{S}(y) + \mu(x) W_0(x)$$

Using this singularity subtraction, the integrand is bounded (but not smooth) and the accuracy of the trapezoid rule improves to $O(h^2)$.

In [2], a method for computing singular integrals is developed that splits the integral into a global part and local part using a floating partition of unity, The local part is evaluated in polar coordinates. For a fixed angle, the resulting integrand is smooth in the radial direction. Furthermore, the radial integral is a smooth function of the angle. Thus, the trapezoid rule is high order accurate provided that the integrand is sampled in polar coordinates. In [2, 10] the remaining global part is integrated to high order using the trapezoid rule on overlapping surface patches.

In this work, we use our high-order quadrature formula given in equation (2.9) to compute the global part rather than the overlapping patch method. Thus, we extend the work in [2] to complicated implicitly defined surfaces for which the overlapping patch method is not practical. As in section 2.6, we assume that ϕ and $\nabla\phi$ are known exactly. For our numerical examples, we evaluate $W_0(x)$, given in equation (3.1), for various $x \in \mathcal{S}$. Thus, in all of our test cases we are computing a singular integral whose exact value is given by $W_0(x) = -2\pi$.

We next describe how to cut the integral $W_0(x)$ into a *global part* and a *local part* using a locally flat cutoff function. Let $\zeta(r)$ be a smooth, even, and non-negative function with support contained in $[-1,1]$ such that $|\zeta(r)| \leq 1$ and $\zeta(r) = 1$ for $r \in [-\eta, \eta]$ for some $\eta \in (0,1)$. See appendix A for a specific example. For a given localization radius $\delta > 0$, set $\zeta_\delta(r) = \zeta(r/\delta)$ and define the localized version of $W_0(x)$ as

$$W_0^L(x) = \int_{\mathcal{S}} \frac{\nu(y) \cdot (x-y)}{|x-y|^3} \zeta_\delta(|x-y|) d\mathcal{S}(y)$$

The remainder is called the *global integral* and is defined

$$W_0^G(x) = W_0(x) - W_0^L(x) = \int_{\mathcal{S}} \frac{\nu(y) \cdot (x-y)}{|x-y|^3} (1 - \zeta_\delta(|x-y|)) d\mathcal{S}(y) \tag{3.2}$$

Because of the local flatness of ζ, the global integrand is exactly zero in a ball centered at the evaluation point x with radius $\eta\delta$. Hence, the global integrand is smooth and can be approximated using our new high-order quadrature formula.

3.1 Numerical Results

For our numerical tests, we compute the local part $W_0^L(x)$ to very high precision using a high-order quadrature method. We use the inverse of the tangent plane projection for our local coordinates. Using a method similar to that described in [10], we sample the integrand in polar coordinates and integrate the angular and radial parts using the trapezoid rule. Because of the high-order convergence of this method, the local integral can quickly be computed to very high accuracy. Because we are working with implicitly defined surfaces, sampling the inverse tangent plane projection involves using Newton's method. To compute the initial guesses, we use a Taylor series approximation of the inverse projection centered at the evaluation point. Using this procedure, we compute the local part to such high accuracy that the local error is orders of magnitude smaller than the global error and thus can be

ignored. Thus, the reported errors for our numerical tests indicate the quadrature error resulting from approximating the global integral given in equation (3.2) using equation (2.9).

3.1.1 Double Torus

In this section, our test surface $\mathcal{S}$ is the double torus whose level set function is given by equation (B.1). We evaluate Gauss's integral at the three evaluation points $\{x^1, x^2, x^2\} \subseteq \mathcal{S}$ which are described in table 3.1. The table also shows the two principal curvatures at the evaluation points. For our numerical tests we use $\delta = 0.1$,

Table 3.1: Evaluation Points : Double Torus

i	x_1^i	x_2^i	x_3^i	κ_1^i	κ_2^i
1	0.62501433494088	0.01	0.01	-6.00	3.81
2	0.89964275194013	0.01	0.01	-4.17	2.66
3	1.19254924926733	0.01	0.01	-0.81	-0.51

$\eta = 1/4$, and $\theta = 63.5°$. The results for each evaluation point x^i are shown in table 3.2 for various values of h.

Table 3.2: Gauss's Integral : Double Torus

$-(\log_2 h)$	i	rel err	order	i	rel err	order	i	rel err	order
7	1	$8.81 \cdot 10^{-5}$		2	$1.94 \cdot 10^{-4}$		3	$1.67 \cdot 10^{-4}$	
8	1	$8.52 \cdot 10^{-6}$	3.37	2	$2.05 \cdot 10^{-5}$	3.24	3	$1.99 \cdot 10^{-5}$	3.08
9	1	$1.40 \cdot 10^{-7}$	5.93	2	$3.82 \cdot 10^{-7}$	5.75	3	$4.27 \cdot 10^{-7}$	5.54
10	1	$6.26 \cdot 10^{-10}$	7.81	2	$1.89 \cdot 10^{-9}$	7.66	3	$2.34 \cdot 10^{-9}$	7.51

3.1.2 Orthocircles

In this section, our test surface $\mathcal{S}$ is the orthocircles surface whose level set function is given by equation (B.2). We evaluate Gauss's integral at the three evaluation

points $\{x^1, x^2, x^2\} \subseteq \mathcal{S}$ which are described in table 3.3. The table also shows the two principal curvatures at the evaluation points. Note that although the evaluation points are close in proximity, the curvature variation is substantial. Furthermore, the maximum absolute curvature at x^3 is very large. These principal curvature samples indicate the high complexity of the orthocircles surface. For our numerical tests we

Table 3.3: Evaluation Points : Orthocircles

i	x_1^i	x_2^i	x_3^i	κ_1^i	κ_2^i
1	0.15741323309941	0.55	0.75	-3.80	1.70
2	0.19926311469040	0.6	0.75	-8.44	1.71
3	0.21749444292873	0.65	0.75	-19.5	1.47

use $\delta = 0.05$, $\eta = 1/4$, and $\theta = 63.5°$. The results for each evaluation point x^i are shown in table 3.4 for various values of h.

Table 3.4: Gauss's Integral : Orthocircles

$-(\log_2 h)$	i	rel err	order	i	rel err	order	i	rel err	order
6	1	$9.00 \cdot 10^{-5}$		2	$7.97 \cdot 10^{-4}$		3	$4.35 \cdot 10^{-4}$	
7	1	$2.04 \cdot 10^{-5}$	2.14	2	$4.28 \cdot 10^{-5}$	4.22	3	$5.50 \cdot 10^{-5}$	2.98
8	1	$5.26 \cdot 10^{-7}$	5.28	2	$1.06 \cdot 10^{-6}$	5.34	3	$2.32 \cdot 10^{-6}$	4.57
9	1	$8.20 \cdot 10^{-10}$	9.32	2	$1.64 \cdot 10^{-8}$	6.02	3	$6.46 \cdot 10^{-9}$	8.49

3.1.3 Tanglecube

In this section, our test surface $\mathcal{S}$ is the tanglecube whose level set function is given by equation (B.3). We evaluate Gauss's integral at the three evaluation points $\{x^1, x^2, x^2\} \subseteq \mathcal{S}$ which are described in table 3.5. The table also shows the two principal curvatures at the evaluation points. For our numerical tests we use $\delta = 0.1$, $\eta = 1/4$, and $\theta = 63.5°$. The results for each evaluation point x^i are shown in table 3.6 for various values of h.

Table 3.5: Evaluation Points : Tanglecube

i	x_1^i	x_2^i	x_3^i	κ_1^i	κ_2^i
1	1.13765711461064	2.1	2.1	-1.84	-0.33
2	1.67841026081049	2.14	2.14	-1.78	-0.95
3	0.96889137698733	0	1.5	-2.58	1.60

Table 3.6: Gauss's Integral : Tanglecube

$-(\log_2 h)$	i	rel err	order	i	rel err	order	i	rel err	order
6	1	$8.25 \cdot 10^{-6}$		2	$4.88 \cdot 10^{-5}$		3	$1.66 \cdot 10^{-5}$	
7	1	$1.50 \cdot 10^{-6}$	2.46	2	$1.27 \cdot 10^{-6}$	5.26	3	$5.09 \cdot 10^{-7}$	5.03
8	1	$4.48 \cdot 10^{-8}$	5.06	2	$2.23 \cdot 10^{-8}$	5.84	3	$3.52 \cdot 10^{-9}$	7.17
9	1	$2.33 \cdot 10^{-11}$	10.91	2	$2.11 \cdot 10^{-10}$	6.72	3	$5.53 \cdot 10^{-12}$	9.32

4

Localized Single Layer Potentials

4.1 Introduction

For an evaluation point $x \in \mathbb{R}^3$, we write a single layer potential as

$$V(x) = \int_{\mathcal{S}} \mu(y) \frac{1}{|x-y|} d\mathcal{S}(y) \tag{4.1}$$

where $\mu : \mathcal{S} \to \mathbb{R}$ is called the density. If $x \in \mathcal{S}$, the integral is weakly singular and a straightforward application of the trapezoid rule to overlapping surface patches is only $O(h)$ accurate where h is the quadrature spacing. In [2], a method for singular integrals is developed that splits the integral into a global part and a local part using a floating partition of unity. The local part is evaluated in polar coordinates. For a fixed angle, the resulting integrand is smooth in the radial direction. Further, the radial integral is a smooth function of the angle. Thus, the trapezoid rule is high order accurate provided that the integrand is sampled in polar coordinates. For a fixed localization radius, the global part is smooth and thus can be integrated to high order using, for example, the trapezoid rule on overlapping patches [2, 10] or the high-order quadrature formula given in equation (2.9).

For evaluation points far off the surface, single layer potentials are smooth and can easily be evaluated using standard high-order quadrature techniques. The more difficult case occurs when the evaluation point is very near the surface. Although the resulting integrands are smooth in the classical sense, the derivatives become very large and standard quadrature techniques achieve very low accuracy. Unlike in the singular case, a near singularity cannot be removed using polar coordinates. Thus, the techniques for evaluating the local integral that work in the singular case cannot be directly applied to the nearly singular case.

In our work, we extend the applicability of the localization method first discussed in [2] to the nearly singular case. We use a novel $O(1)$ algorithm to approximate the local part of a singular or nearly singular integral. Because of the efficiency advantage of our method, we improve on the approach given in [2] for the singular case as well. Although we restrict our attention to the single layer potential given by equation (4.1), our method can easily be extended to other integrals such as the double layer potential. Previous methods to tackle nearly singular integrals include kernel smoothing with corrections [1] and interpolation [10]. The work in [1] applies to both singular and nearly singular integrals.

In this chapter, we consider the approximation of a single layer potential in the case where the integrand has been localized to a small ball with radius δ centered at the evaluation point x. We consider both singular and nearly singular integrals. As in [10], we use a locally flat cutoff function for the localization. We make a key use of the local flatness in our treatment of the nearly singular case. To perform the local integration, we use a local projection onto the tangent plane at x and then write the integral in polar coordinates. We consider the angular integral and the radial integral separately.

We first prove the surprising fact that the angular integral can be approximated very accurately using the trapezoid rule with only a few angular samples of the radial

integral. Our proof technique uses a key aspect of our choice of local coordinates, specifically the projection onto the tangent plane, to show that the radial integral can be well approximated by a low degree trigonometric polynomial which is integrated *exactly* by the trapezoid rule with a small number of quadrature points.

After using the trapezoid rule to approximate the angular integral, we are left with a small number of radial integrals to compute. We first show that by multiplying the integrands by certain helper functions and using a change of variable, the radial integrals can be written in terms of standard integrals that can be precomputed and stored in a lookup table. Since the helper functions are chosen to be close to the identity, the remainder terms are small. By keeping track of the remainder terms using a recurrence relation, we develop a formula for approximating the radial integrals to high order. The formula depends on derivatives of certain recursively defined functions which are estimated using centered finite differences on a small radial grid.

Using our angular and radial integration methods, the local integral can be approximated to high order in δ using $O(1)$ steps. Given that a typical application of potential theory requires a very large number of local integral calculations, our method should have an efficiency advantage over previous fully numerical methods, such as described in [10], that require $O(1/\delta^2)$ quadrature points to approximate the local part of a singular integral to high order. Our method has the additional advantage of working for both singular and nearly singular integrals. Thus, we extend the applicability of the localization approach to general single layer potentials. Finally, because of the small number of coordinate function samples required, our method has an efficiency advantage in situations where the surface is given implicitly and sampling the coordinate functions requires an iterative root finding method.

In the remainder of this section, we first explain our localization technique, and then describe the integral in certain local coordinates using a height function. Next,

we give algorithms for sampling the height function and its derivatives in the case where $\mathcal{S}$ is implicitly defined. Finally, we switch to polar coordinates and show how to remove the boundary at $r = 0$ in the radial integral. In section 4.2, we give brief descriptions of our angular and radial integration methods as well as our combined local integration method. In section 4.3, we prove an approximation theorem which is the theoretical foundation of our angular integration method. In sections 4.4, 4.5, and 4.6 we give a detailed treatment of the radial integral formula which we use to evaluate the radial integrals.

In the final two sections, we present the numerical results for our local integration methods. We consider both singular and nearly singular integrals. In section 4.7, we numerically verify the predicted convergence rates of the angular and radial integration methods in isolation and then together in a combined test. In section 4.8, we numerically verify the accuracy of our $O(1)$ local integration method on two complex implicitly defined surfaces with various evaluation points.

4.1.1 Localization

We next describe how to cut the integral $V(x)$ into a *global part* and a *local part* using a locally flat cutoff function. Let $\zeta(r)$ be a smooth, even, and non-negative function with support contained in $[-1, 1]$ such that $|\zeta(r)| \leq 1$ and $\zeta(r) = 1$ for $r \in [-\eta, \eta]$ for some $\eta \in (0, 1)$. See appendix A for a specific example. For a given localization radius $\delta > 0$, set $\zeta_\delta(r) = \zeta(r/\delta)$ and define the localized version of $V(x)$ as

$$V^L(x) = \int_{\mathcal{S}} \mu(y) \frac{1}{|x - y|} \zeta_\delta(|x - y|) d\mathcal{S}(y) \tag{4.2}$$

The remainder is called the global integral and is defined

$$V^G(x) = V(x) - V^L(x) = \int_{\mathcal{S}} \mu(y) \frac{1}{|x - y|} (1 - \zeta_\delta(|x - y|)) d\mathcal{S}(y)$$

Because of the local flatness of ζ, the global integrand is exactly zero in a ball centered at the evaluation point x with radius $\eta\delta$. Thus, for a fixed δ, the global integral is smooth and can be integrate to high order using, for example, the trapezoid rule on overlapping surface patches [2, 10]. As in the case of the double layer potential, see chapter 3, the global part can also be integrated with high-order convergence using equation (2.9) developed in section 2.1.

In this chapter, we focus on the the high-order evaluation of the local integral $V^L(x)$ given be equation (4.2).

4.1.2 Local Coordinates

We wish to compute $V^L(x)$ for $x \in \mathcal{S}$ and x near $\mathcal{S}$. Given x on or near $\mathcal{S}$, let $x_p \in \mathcal{S}$ be the point on the surface with the minimum distance to x and define $x_n = x - x_p$. We assume that δ is chosen small enough so that $\{y \in \mathcal{S} : \zeta_\delta(|x-y|) \neq 0\}$ can be smoothly projected onto the tangent plane at x. We assume coordinates such that $x_p = (0,0,0)$, $x_n = (0,0,\gamma)$, and $\nu(x_p) = (0,0,1)$ where $\nu(x_p)$ is the unit normal at x_p. Note that $|\gamma| = |x_n| = |x - x_p|$ is the distance between x and the surface $\mathcal{S}$. We use the coordinate mapping $\Phi(s,t) = (s,t,Z(s,t))$ where Z denotes the height. Note that $Z(0,0) = Z_s(0,0) = Z_t(0,0) = 0$, the area element is $|\Phi_s \times \Phi_t| = (1+Z_s^2+Z_t^2)^{1/2}$, and $|x-y| = (s^2+t^2+(Z-\gamma)^2)^{1/2}$. Writing

$$F(s,t) = \mu(\Phi(s,t))(1+Z_s^2+Z_t^2)^{1/2} \tag{4.3}$$

we see that

$$V^L(x) = \int_{-\delta}^{\delta}\int_{-\delta}^{\delta} \frac{F(s,t)}{(s^2+t^2+(Z(s,t)-\gamma)^2)^{1/2}} \zeta_\delta((s^2+t^2+(Z(s,t)-\gamma)^2)^{1/2}) ds dt$$

4.1.3 Height Function Sampling and Implicitly Defined Surfaces

To compute a localized single layer potential $V^L(x)$ using our $O(1)$ algorithm, we will need to sample the local coordinate height function $Z(s,t)$ (see section 4.1.2)

as well as the functions $Z_s(s,t)$, $Z_t(s,t)$ and $F(s,t)$. Let $\mathcal{S} \subseteq \mathbb{R}^3$ be a compact smooth implicitly defined surface with global defining function ϕ. We assume that the density μ as well as ϕ and $\nabla\phi$ are known.

Let $x = x_n + x_p$ be an evaluation point where $x_p \in \mathcal{S}$ is the point on $\mathcal{S}$ with minimum distance to x. Let $M = (u, v, w)$ be an orthogonal matrix with $w = \nu(x_p)$. Define

$$\psi(y) = \phi(My + x_p) \tag{4.4}$$

and note that

$$\nabla\psi(y) = M^t(\nabla\phi(My + x_p)) \tag{4.5}$$

The height function $Z(s,t)$ satisfies

$$\psi(s,t,Z(s,t)) = 0 \tag{4.6}$$

for sufficiently small s and t. To sample $Z(s,t)$, we set $g(a) = \psi(s,t,a)$ and find a root using Newton's method. Since $Z(0,0) = Z_s(0,0) = Z_t(0,0) = 0$ we have that $Z(s,t) = O(s^2 + t^2)$ and thus we use $a^0 = 0$ as our initial guess. We use equations (4.4) and (4.5) to evaluate $g(a)$ and $g'(a)$ for Newton's method.

Differentiating equation (4.6) with respect to s gives

$$\psi_1(s,t,Z(s,t)) + \psi_3(s,t,Z(s,t))Z_s(s,t) = 0$$

Similarly, Differentiating equation (4.6) with respect to t gives

$$\psi_2(s,t,Z(s,t)) + \psi_3(s,t,Z(s,t))Z_t(s,t) = 0$$

Our algorithm for computing $Z(s,t)$, $Z_s(s,t)$ and $Z_t(s,t)$ is thus as follows.

1. Compute $Z(s,t)$ using Newton's method on $g(a) = \psi(s,t,a)$ with an initial guess of $a^0 = 0$.

2. Set $y = (s,t,Z(s,t))$ and compute $G = \nabla\psi(y)$ using equation (4.5).

3. Set $Z_s(s,t) = -G_1/G_3$ and $Z_t(s,t) = -G_2/G_3$.

Once we have Z, Z_s and Z_t, we compute F using the density μ and equation (4.3).

4.1.4 The Angular Function and Polar Coordinates

We define the the *angular function* as

$$A(\theta,\delta,\gamma) = \int_0^\delta \frac{rf(r,\theta)}{(r^2+(z(r,\theta)-\gamma)^2)^{1/2}}\zeta_\delta((r^2+(z(r,\theta)-\gamma)^2)^{1/2})dr \tag{4.7}$$

where we set $f(r,\theta) = F(r\cos\theta, r\sin\theta)$ and $z(r,\theta) = Z(r\cos\theta, r\sin\theta)$. In polar coordinates the localized single layer potential is thus

$$V^L(x) = \int_0^{2\pi} A(\theta,\delta,\gamma)d\theta$$

It is sometimes more convenient to compute the radial integral

$$B(\theta,\delta,\gamma) = A(\theta,\delta,\gamma) + A(\theta+\pi,\delta,\gamma) \tag{4.8}$$

instead of $A(\theta,\delta,\gamma)$. Noting that $f(r,\theta+\pi) = f(-r,\theta)$ and $z(r,\theta+\pi) = z(-r,\theta)$, we substitute $r = -r$ and switch the integration limits to see that

$$A(\theta+\pi,\delta,\gamma) = \int_{-\delta}^0 \frac{-rf(r,\theta)}{(r^2+(z(r,\theta)-\gamma)^2)^{1/2}}\zeta_\delta((r^2+(z(r,\theta)-\gamma)^2)^{1/2})dr$$

Because $|r| = r$ for $r \geq 0$ and $|r| = -r$ for $r \leq 0$ we have by equation (4.8),

$$B(\theta,\delta,\gamma) = \int_{-\delta}^\delta \frac{|r|f(r,\theta)}{(r^2+(z(r,\theta)-\gamma)^2)^{1/2}}\zeta_\delta((r^2+(z(r,\theta)-\gamma)^2)^{1/2})dr \tag{4.9}$$

Since

$$\int_0^{2\pi} A(\theta,\delta,\gamma) = \int_0^\pi A(\theta,\delta,\gamma)d\theta + \int_0^\pi A(\theta+\pi,\delta,\gamma)d\theta = \int_0^\pi B(\theta,\delta,\gamma)d\theta \tag{4.10}$$

we have the following alternate form of the localized single layer potential

$$V^L(x) = \int_0^\pi B(\theta,\delta,\gamma)d\theta \tag{4.11}$$

4.2 Overview of Local Integration Method

In this section, we give brief descriptions of our angular and radial integration methods as well as our combined local integration method.

4.2.1 The Angular Integral

Since $B(\theta, \delta, \gamma)$ is π-periodic, it is natural to use the trapezoid rule to estimate the angular integral part of $V^L(x)$ given in equation (4.11). For $n > 0$, set $h = \pi/n$ and $\theta_i = ih$. The trapezoid rule approximation of $V^L(x)$ is

$$V_h^L(x) = \sum_{i=0}^{n-1} B(\theta_i, \delta, \gamma)h \tag{4.12}$$

It is well known that the trapezoid rule is very accurate when used to integrate a smooth periodic function over a complete period. The trapezoid rule has been used to approximate the angular part of localized singular integrals in prior work with excellent results [2, 10]. However, the nearly singular case was not considered. Our numerical evidence (see section 4.7.1) suggests that the convergence of the angular integral approximation is very rapid for both the singular and nearly singular cases. One interesting aspect illuminated by the numerical tests is that the approximation converges rapidly as $\delta \to 0$ for a fixed h. This suggests that the standard analysis based on the Euler-Maclaurin formula applied to periodic functions does not provide a complete understanding of the convergence. In section 4.3 we prove that the angular integral approximation convergences rapidly as $\delta \to 0$ with a fixed number of quadrature points. The main idea of the proof is to exploit our choice of local coordinates to show that the angular function $A(\theta, \delta, \gamma)$ can be well approximated by low-degree trigonometric polynomials which are integrated exactly by the trapezoid rule with a small number of quadrature points.

Recall that a trigonometric polynomial of degree at most N is a function of the

form

$$T(\theta) = a_0 + \sum_{n=1}^{N} a_n \cos(n\theta) + \sum_{n=1}^{N} b_n \sin(n\theta)$$

In section 4.3 we prove the following approximation theorem.

Theorem 11. *Let $\delta' > 0$. Assume $F(s,t) \in C^\infty([-\delta',\delta']^2)$, $Z(s,t) \in C^\infty([-\delta',\delta']^2)$, and that $Z(0,0) = Z_s(0,0) = Z_t(0,0) = 0$. Set $f(r,\theta) = F(r\cos\theta, r\sin\theta)$ and $z(r,\theta) = Z(r\cos\theta, r\sin\theta)$ and define $A(\theta,\delta,\gamma)$ using equation (4.7). Then, for all $m \geq 0$ there exists a trigonometric polynomial $T(\theta,\delta,\gamma)$ of degree at most $4m+1$ and constants C_1 and C_2 such that*

$$|A(\theta,\delta,\gamma) - T(\theta,\delta,\gamma)| \leq C_1\delta^{2m+3} + C_2|\gamma|\delta^{2m+1}$$

for all $\theta \in [0,2\pi]$, $\delta \leq \delta'$, and $\gamma \in [-\delta,\delta]$.

One corollary of the approximation theorem, see corollary 14, is that for all $m \geq 0$ we have

$$\left| \int_0^\pi B(\theta,\delta,\gamma)d\theta - \sum_{j=0}^{2m} B(\theta_j,\delta,\gamma)h \right| = O(\delta^{2m+3}) + O(|\gamma|\delta^{2m+1}) \tag{4.13}$$

Thus, our $O(1)$ method for approximating the angular integral part of $V^L(x)$ given in equation (4.11), is to pick an $m \geq 0$ and use the trapezoid rule approximation given in equation (4.12) with $n = 2m+1$. By equation (4.13), the order of our approximation method for the angular integral is $O(\delta^{2m+3}) + O(|\gamma|\delta^{2m+1})$.

4.2.2 The Radial Integral

The goal of our radial integral method is to estimate the radial integral

$$\int_{-\delta}^{\delta} \frac{|r|f(r,\theta)}{(r^2 + (z(r,\theta)-\gamma)^2)^{1/2}} \zeta_\delta((r^2 + (z(r,\theta)-\gamma)^2)^{1/2})dr \tag{4.14}$$

to high order in δ for a fixed angle θ'. For a fixed θ', the functions $f(r,\theta')$ and $z(r,\theta')$ are functions of r alone. For brevity of exposition, we define $f(r) = f(r,\theta')$ and $z(r) = z(r,\theta')$ and consider the computation of the following one-dimensional integral

$$I(\delta,\gamma) = \int_{-\delta}^{\delta} \frac{|r| f(r)}{(r^2 + (z(r)-\gamma)^2)^{1/2}} \zeta_\delta((r^2 + (z(r)-\gamma)^2)^{1/2}) dr \tag{4.15}$$

where we assume as usual that $f, z \in C^\infty[-\delta', \delta']$ for some constant $\delta' > 0$ and that $z(0) = z'(0) = 0$. For simplicity, we assume that $\gamma = O(\delta^2)$ and leave the more general case for future research. Note that this assumption regarding γ is only used in section 4.6. It is *not* needed for the results in sections 4.4 and 4.5.

To estimate the radial integral, we pick $m \geq 0$ and use the estimation algorithm in section 4.6.5. The key ingredient of the estimation algorithm is the radial integral formula given by equation (4.58) which is derived in section 4.4. The radial integrals, $\Lambda_{2k}(\beta)$, in equation (4.58) are evaluated in terms of standard precomputed radial integrals using the formulas given in section 4.5. Finally, the remaining terms in the radial integral formula are estimated using the algorithms given in section 4.6. The estimation algorithms use the $(2m+1)$-point centered finite difference formulas (see section 4.6.2) applied to $2m+1$ regularly spaced samples of the input functions f, z, and z_r (see section 4.6.3 for details). The theory developed in sections 4.4, 4.5, and 4.6 show that the overall error in our radial integral estimation algorithm is $O(\delta^{2m+3})$.

4.2.3 The Combined Local Integral

To estimate a local single layer potential given by equation (4.11), we pick $m \geq 0$ and use that choice of m for both the angular and radial integration methods described above. For the combined method we assume that $\gamma = O(\delta^2)$. Thus, for a given $m \geq 0$, the order of the angular method is $O(\delta^{2m+3})$ and the order of the radial

method is $O(\delta^{2m+3})$. By the triangle inequality, the order of the combined method is also $O(\delta^{2m+3})$. Note that our combined approximation method uses $(2m+1)(2m)+1$ sample points of the functions f, z, and z_r. More specifically, there are $(2m+1)$ angular samples and for each angular sample we need $(2m+1)$ radial points but the middle radial point is the same for each angular sample. In the implicitly defined surface case, the input samples of f, z, and z_r are computed using samples of F, Z, Z_s, and Z_t found using the method in section 4.1.3. This method only requires knowledge of μ, ϕ and $\nabla\phi$ where μ is the density and ϕ is the global defining function for the implicitly defined surface.

Thus, for a given $m \geq 0$ our local integration method does a constant amount of work and has an overall $O(\delta^{2m+3})$ error.

4.3 The Angular Function Approximation Theorem

In this section we prove the quadrature corollaries and the angular function approximation theorem which establish the theoretical foundation of our angular integral approximation method.

4.3.1 Corollaries of the Approximation Theorem

Before proceeding to the proof of the angular function approximation theorem, we give the main applications which are the quadrature corollaries. We start by proving a well known exactness property of the trapezoid rule.

Lemma 12. *Let $h = 2\pi/N$ and $\theta_j = jh$ and suppose that $T(\theta)$ is a trigonometric polynomial of degree $n < N$. Then we have that*

$$\int_0^{2\pi} T(\theta)d\theta = \sum_{j=0}^{N-1} T(\theta_j)h$$

Proof. Recall that a trigonometric polynomial of degree n can be written as

$$T(\theta) = \sum_{k=-n}^{n} c_k e^{ik\theta}$$

where $c_k \in \mathbb{C}$. Since $\int_0^{2\pi} e^{ik\theta} = 0$ for all $k \neq 0$ and the trapezoid rule is exact for constants, it suffices to note that for all $k \neq 0$ such that $|k| < N$ we have

$$\sum_{j=0}^{N-1} e^{ik\theta_j} = \sum_{j=0}^{N-1} \left(e^{\frac{i2\pi k}{N}}\right)^j = \frac{1 - e^{i2\pi k}}{1 - e^{\frac{i2\pi k}{N}}} = 0$$

□

The first corollary allows us to reduce the problem of computing $\int_0^{2\pi} A(\theta, \delta, \gamma) d\theta$ to that of computing the radial integrals $A(\theta, \delta, \gamma)$ defined by equation (4.7) for a small number of angular samples $\{\theta_j\}$. The parameter ω is needed for the proof of corollary 14.

Corollary 13. *Let $\delta' > 0$ and $m \geq 0$. Assume that $F(s,t) \in C^\infty([-\delta', \delta']^2)$, $Z(s,t) \in C^\infty([-\delta', \delta']^2)$, and that $Z(0,0) = Z_s(0,0) = Z_t(0,0) = 0$. Set $h = 2\pi/(4m+2)$ and $\theta_j = jh$. Then there exist constants C_1 and C_2 such that*

$$\left| \int_0^{2\pi} A(\theta + \omega, \delta, \gamma) d\theta - \sum_{j=0}^{4m+1} A(\theta_j + \omega, \delta, \gamma) h \right| \leq C_1 \delta^{2m+3} + C_2 |\gamma| \delta^{2m+1}$$

for all $\delta \leq \delta'$, $\gamma \in [-\delta, \delta]$, and $\omega \in [0, 2\pi]$.

Proof. By theorem 11, there exists a trigonometric polynomial $T(\theta, \delta, \gamma)$ of degree at most $4m+1$ and constants C_1' and C_2' such that

$$|A(\theta, \delta, \gamma) - T(\theta, \delta, \gamma)| \leq C_1' \delta^{2m+3} + C_2' |\gamma| \delta^{2m+1} \tag{4.16}$$

for all $\theta \in [0, 2\pi]$, $\delta \leq \delta'$ and $\gamma \in [-\delta, \delta]$. Note that $T(\theta + \omega, \delta, \gamma)$ is also a trigonometric polynomial of degree at most $4m + 1$ and thus by lemma 12,

$$\int_0^{2\pi} T(\theta + \omega, \delta, \gamma) d\theta = \sum_{j=0}^{4m+1} T(\theta_j + \omega, \delta, \gamma) h$$

By the triangle inequality and equation (4.16) we have

$$\left| \int_0^{2\pi} A(\theta + \omega, \delta, \gamma) d\theta - \sum_{j=0}^{4m+1} A(\theta_j + \omega, \delta, \gamma) h \right|$$

$$\leq \int_0^{2\pi} |A(\theta + \omega, \delta, \gamma) - T(\theta + \omega, \delta, \gamma)| d\theta + h \sum_{j=0}^{4m+1} |A(\theta_j + \omega, \delta, \gamma) - T(\theta_j + \omega, \delta, \gamma)|$$

$$\leq (C_1' \delta^{2m+3} + C_2' |\gamma| \delta^{2m+1}) \left(\int_0^{2\pi} d\theta + h \sum_{j=0}^{4m+1} 1 \right) = 4\pi (C_1' \delta^{2m+3} + C_2' |\gamma| \delta^{2m+1})$$

□

The next corollary gives the analogous result for integrating $\int_0^{\pi} B(\theta, \delta, \gamma) d\theta$.

Corollary 14. *Let $\delta' > 0$ and $m \geq 0$. Assume that $F(s, t) \in C^{\infty}([-\delta', \delta']^2)$, $Z(s, t) \in C^{\infty}([-\delta', \delta']^2)$, and that $Z(0, 0) = Z_s(0, 0) = Z_t(0, 0) = 0$. Set $h = \pi/(2m + 1)$ and $\theta_j = jh$. Then there exist constants C_1 and C_2 such that*

$$\left| \int_0^{\pi} B(\theta, \delta, \gamma) d\theta - \sum_{j=0}^{2m} B(\theta_j, \delta, \gamma) h \right| \leq C_1 \delta^{2m+3} + C_2 |\gamma| \delta^{2m+1} \tag{4.17}$$

for all $\delta \leq \delta'$ and all $\gamma \in [-\delta, \delta]$.

Proof. We apply corollary 13 with $\omega = 0$ and $\omega = \pi$ to see that

$$\left| \int_0^{2\pi} A(\theta, \delta, \gamma) d\theta - \sum_{j=0}^{4m+1} A(\theta_j, \delta, \gamma) h \right| \leq C_1 \delta^{2m+3} + C_2 |\gamma| \delta^{2m+1} \tag{4.18}$$

$$\left| \int_0^{2\pi} A(\theta + \pi, \delta, \gamma) d\theta - \sum_{j=0}^{4m+1} A(\theta_j + \pi, \delta, \gamma) h \right| \leq C_1 \delta^{2m+3} + C_2 |\gamma| \delta^{2m+1} \tag{4.19}$$

Using the triangle inequality and equations (4.18) and (4.19), we compute

$$\left| \int_0^{2\pi} B(\theta, \delta, \gamma) d\theta - \sum_{j=0}^{4m+1} B(\theta_j, \delta, \gamma) h \right| \leq 2(C_1 \delta^{2m+3} + C_2 |\gamma| \delta^{2m+1})$$

Finally, because $B(\theta, \delta, \gamma)$ is π-periodic we have that

$$\left| \int_0^{\pi} B(\theta, \delta, \gamma) d\theta - \sum_{j=0}^{2m} B(\theta_j, \delta, \gamma) h \right| \leq C_1 \delta^{2m+3} + C_2 |\gamma| \delta^{2m+1}$$

□

4.3.2 Preliminary Analysis

Before proving the approximation theorem, we take care of some preliminary analysis. We frequently encounter functions of the form $h(r, \theta) = H(r \cos\theta, r \sin\theta)$ where $H(s, t) \in C^\infty([-\delta', \delta']^2)$ and will need to use Taylor analysis in the radial variable r. Our first lemma deals with the derivatives of $h(r, \theta)$ in the r variable.

Lemma 15. *Let $\delta' > 0$ and assume that $H(s, t) \in C^k([-\delta', \delta']^2)$. Define $h(r, \theta) = H(r \cos\theta, r \sin\theta)$. Then there exist constants $\{C_{i,j}\}_{i+j=k}$ such that for all $r \in [0, \delta']$ and all $\theta \in [0, 2\pi]$ we have*

$$h^{(k)}(r, \theta) = \sum_{i+j=k} C_{i,j} \cos^i(\theta) \sin^j(\theta) H^{(i,j)}(r \cos\theta, r \sin\theta) \tag{4.20}$$

where $h^{(k)}$ is the k^{th} derivative in the r variable and $H^{(i,j)} = \frac{\partial^{i+j} H}{\partial s^i \partial t^j}$. Furthermore, we have

$$\left| h^{(k)}(r, \theta) \right| \leq \sum_{i+j=k} |C_{i,j}| H_{i,j} \tag{4.21}$$

for all $r \in [0, \delta']$ and $\theta \in [0, 2\pi]$ where $H_{i,j} = \max_{(s,t) \in [-\delta', \delta']^2} |H^{(i,j)}(s, t)|$.

Proof. Differentiating $C_{i,j}\cos^i(\theta)\sin^j(\theta)H^{(i,j)}(r\cos\theta, r\sin\theta)$ in r gives

$$C_{i,j}\cos^{i+1}(\theta)\sin^j(\theta)H^{(i+1,j)}(s,t) + C_{i,j}\cos^i(\theta)\sin^{j+1}(\theta)H^{(i,j+1)}(s,t)$$

where $s = r\cos\theta$ and $t = r\sin\theta$. Thus $h^{(k+1)}(r,\theta)$, which is the sum of such derivatives, can be put into the form of equation (4.20) and the first part follows by induction on k. The second part is an application of equation (4.20) and the continuity of $H^{(i,j)}(s,t)$. □

The next two lemmas show how trigonometric polynomials arise when studying $h(r,\theta)$.

Lemma 16. *Let $g(\theta) = \cos^i(\theta)\sin^j(\theta)$ where $i \geq 0$ and $j \geq 0$. Then $g(\theta)$ is a trigonometric polynomial of degree at most $i + j$.*

Proof. We use induction on $i + j$. The case where $i + j = 0$ is trivial. For the inductive step assume that $i > 0$ the other case being similar. By the inductive hypothesis, $g(\theta) = T(\theta)\cos(\theta)$ where $T(\theta)$ is a trigonometric polynomial of degree at most $i - 1 + j$. Since $n \leq i - 1 + j$, the product-to-sum formulas,

$$a_n\cos(n\theta)\cos(\theta) = \frac{a_n}{2}\left(\cos((n-1)\theta) + \cos((n+1)\theta)\right)$$

$$b_n\sin(n\theta)\cos(\theta) = \frac{b_n}{2}\left(\sin((n+1)\theta) + \sin((n-1)\theta)\right)$$

show that $T(\theta)\cos(\theta)$ is a trigonometric polynomial of degree at most $i + j$. □

Lemma 17. *Let $\delta' > 0$ and assume that $H(s,t) \in C^k([-\delta', \delta']^2)$. Define $h(r,\theta) = H(r\cos\theta, r\sin\theta)$. Then $h^{(k)}(0,\theta)$ is a trigonometric polynomial of degree at most k.*

Proof. Plugging $r = 0$ into equation (4.20) shows that

$$h^{(k)}(0,\theta) = \sum_{i+j=k} C_{i,j}\cos^i(\theta)\sin^j(\theta)H^{(i,j)}(0,0)$$

Thus, $h^{(k)}(0,\theta)$ is a linear combination of the trigonometric functions $\{\cos^i(\theta)\sin^j(\theta) : i+j=k\}$. This fact combined with lemma 16 shows that $h^{(k)}(0,\theta)$ is a trigonometric polynomial of degree at most k. $\square$

We next define and study the generic single layer integrand defined for all $x \in [0,1]$ and $R \in (0,1]$ as

$$g(x,R) = \frac{R}{(R^2+x)^{1/2}}\zeta((R^2+x)^{1/2}) \tag{4.22}$$

In the next lemma we examine the k^{th} derivative in the variable x which we denote $g^{(k)}(x,R)$.

Lemma 18.

$$g^{(k)}(x,R) = \sum_{i=0}^{k} \frac{C_i R}{(R^2+x)^{\frac{2k+1-i}{2}}}\zeta^{(i)}((R^2+x)^{1/2}) \tag{4.23}$$

for some constants $\{C_i\}_{0\le i\le k}$. *Furthermore,*

$$|R^{2k}g^{(k)}(x,R)| \le \sum_{i=0}^{k} C_i Z_i R^i$$

for all $R \in (0,1]$ *and* $x \ge 0$ *where* $Z_i = \max_{R\in[0,1]} |\zeta^{(i)}(R)|$. *Finally, we have*

$$\lim_{R\to 0} R^{2k}g^{(k)}(0,R) = \zeta(0)$$

Proof. We assume that equation (4.23) holds for k and prove it for $k+1$. Let $0 \le i \le k$ be arbitrary. We define

$$h(x) = \frac{C_i R}{(R^2+x)^{\frac{2k+1-i}{2}}}\zeta^{(i)}((R^2+x)^{1/2})$$

and compute

$$h'(x) = \frac{C_i(-(2k+1-i)/2)R}{(R^2+x)^{\frac{2(k+1)+1-i}{2}}}\zeta^{(i)}((R^2+x)^{1/2})$$

$$+\frac{C_i(1/2)R}{(R^2+x)^{\frac{2(k+1)+1-(i+1)}{2}}}\zeta^{(i+1)}((R^2+x)^{1/2})$$

which proves the first part. For the second part we use equation (4.23) and note that

$$|R^{2k}g^{(k)}(x,R)| \leq \left|\sum_{i=0}^{k}\frac{C_iR^{2k+1}}{(R^2+x)^{\frac{2k+1-i}{2}}}\zeta^{(i)}((R^2+x)^{1/2})\right| \leq \sum_{i=0}^{k}C_iZ_iR^i$$

For the third part, we multiply equation (4.23) by R^{2k}, plug in $x=0$, and then take the limit as $R\to 0$. □

The third part of lemma 18 shows that $R^{2k}g^{(k)}(0,R)$ has a removable singularity at $R=0$. Hence $R^{2k}h^{(k)}(x,R)$ can be extended to a continuous function for all $(x,R)\in[0,1]^2$.

4.3.3 Proof of the Approximation Theorem

In this section we prove theorem 11. We want to determine how the integral

$$I=\int_0^{\delta}\frac{rf(r,\theta)}{(r^2+(z(r,\theta)-\gamma)^2)^{1/2}}\zeta_{\delta}((r^2+(z(r,\theta)-\gamma)^2)^{1/2})dr$$

varies as a function of θ. We first rescale the radial variable to make the dependence on δ easier to keep track of. By substituting $R=r/\delta$ we see that

$$I=\delta\int_0^{1}\frac{Rf(R\delta,\theta)}{(R^2+(z(R\delta,\theta)-\gamma)^2/\delta^2)^{1/2}}\zeta((R^2+(z(R\delta,\theta)-\gamma)^2/\delta^2)^{1/2})dR$$

The basic idea of the proof is to note that $(z^2(R\delta,\theta)-2\gamma z(R\delta,\theta))/\delta^2=O(|\gamma|+\delta^2)$ which is much smaller than $R^2=O(1)$. Thus, we can use Taylor's theorem to move the θ dependence from the denominator and from the argument of the cutoff function to the numerator where it is easier to analyze.

To facilitate this procedure we use the generic single layer integrand $g(x,R)$ defined by equation (4.22). We note that

$$I=\delta\int_0^{1}f(R\delta,\theta)g\left(x(R\delta,\theta)/\delta^2+\beta^2,R\right)dR \tag{4.24}$$

where

$$x(r,\theta) = z^2(r,\theta) - 2\gamma z(r,\theta), \qquad \beta = |\gamma|/\delta \tag{4.25}$$

For $m \geq 0$, Taylor's theorem implies

$$g(x+\beta^2, R) = \sum_{i=0}^{2m} g^{(i)}(\beta^2, R)\frac{x^i}{i!} + g^{(2m+1)}(x^*, R)\frac{x^{2m+1}}{(2m+1)!} \tag{4.26}$$

where x^* is a number between β^2 and $x+\beta^2$. Next, we plug $x = x(R\delta,\theta)/\delta^2$ into equation (4.26) and plug the result into equation (4.24).

We first consider the remainder term given by

$$I_{2m+1} = \delta \int_0^1 f(R\delta,\theta) g^{(2m+1)}(x^*(R\delta,\theta), R)\frac{x^{2m+1}(R\delta,\theta)}{(2m+1)!\delta^{4m+2}} dR \tag{4.27}$$

where $x^*(R\delta,\theta)$ is a number between β^2 and $x(R\delta,\theta)/\delta^2+\beta^2$. Since $x(R\delta,\theta)/\delta^2+\beta^2 = (z(R\delta,\theta)-\gamma)^2/\delta^2 \geq 0$ we have that $x^*(R\delta,\theta) \geq 0$ for all $R \in [0,1]$ and $\theta \in [0,2\pi]$. By continuity of $F(s,t)$, there exists a C_1 such that $|f(R\delta,\theta)| \leq C_1$ for all $R \in [0,1]$ and $\theta \in [0,2\pi]$. Since $Z(0,0) = Z_s(0,0) = Z_t(0,0)$, lemma 15 and Taylor's theorem proves the existence of a constant C_2 such that $|z(R\delta,\theta)| \leq C_2 R^2\delta^2$ for all $R \in [0,1]$ and $\theta \in [0,2\pi]$. By lemma 18 we further note that

$$|R^{4m+2} g^{(2m+1)}(x^*(R\delta,\theta), R)| \leq C_3$$

for some constant C_3. Using equation (4.25) we compute

$$\frac{|x(R\delta,\theta)|^{2m+1}}{\delta^{4m+2}} \leq (C_2^2 R^4\delta^2 + 2|\gamma|C_2R^2)^{2m+1} \leq C_4\delta^{2m+2} + C_5|\gamma|^{2m+1}$$

for some constants C_4 and C_5 by the binomial theorem. Plugging all of these estimates into equation (4.27) and using the fact that $|\gamma| \leq \delta$ gives

$$|I_{2m+1}| \leq C_{2m+1}\delta^{2m+3} + C'_{2m+1}|\gamma|\delta^{2m+1} \tag{4.28}$$

for some constants C_{2m+1} and C'_{2m+1} that do not depend on θ, δ, or γ.

Next we consider for some arbitrary $i \in \{0, \ldots, 2m\}$ the term

$$I_i = \delta \int_0^1 f(R\delta, \theta) g^{(i)}(\beta^2, R) \frac{x^i(R\delta, \theta)}{i! \delta^{2i}} dR \tag{4.29}$$

First note that by equation (4.25) and the binomial theorem,

$$\frac{x^i(R\delta, \theta)}{i!} = \sum_{j=0}^{i} C_{i,j} \gamma^j z^{2i-j}(R\delta, \theta)$$

where $C_{i,j}$ are constants that depend only on i and j. Next, define $H_{i,j}(s,t) = F(s,t) Z^{2i-j}(s,t)$ and $h_{i,j}(r,\theta) = H_{i,j}(r\cos\theta, r\sin\theta)$. By Taylor's theorem applied in the r variable we have

$$\begin{aligned} h_{i,j}(r,\theta) = & \sum_{k=0}^{2(m+i)-j+1-a(j)} h_{i,j}^{(k)}(0,\theta) \frac{r^k}{k!} \\ & + h_{i,j}^{(2(m+i)-j+2-a(j))}(r^*, \theta) \frac{r^{2(m+i)-j+2-a(j)}}{(2(m+i)-j+2-a(j))!} \end{aligned} \tag{4.30}$$

where r^* is between 0 and r. and $a(j) = 1$ if $j > 0$ and 0 otherwise. We next check to make sure the remainder terms contribute a small error.

We start with the $j = 0$ case in which $a(j) = 0$. A typical remainder term is given by

$$I_{i,0} = C^*_{i,0} \delta^{1-2i} \int_0^1 g^{(i)}(\beta^2, R) h_{i,0}^{(2(m+i)+2))}(r^*, \theta) (R\delta)^{2(m+i)+2)} dR$$

where $C^*_{i,0}$ is a constant. Since $r^* \in [0, \delta']$, lemma 15 implies $|h_{i,0}^{(2(m+i)+2))}(r^*, \theta)| \leq C_1$ for all $\theta \in [0, 2\pi]$. By lemma 18, $R^{2i} g^{(i)}(\beta^2, R) \leq C_2$. Because $2m + 2 \geq 0$, we have $R^{2m+2} \leq 1$. Putting these estimates together we get

$$|I_{i,0}| \leq C^*_{i,0} C_1 C_2 \delta^{(2m+2i+2-2i+1)} = C\delta^{2m+3} \tag{4.31}$$

for some constant C independent of θ, δ, and γ.

Next, consider the $j > 0$ case in which $a(j) = 1$. A typical remainder term is given by

$$I_{i,j} = C^*_{i,j}\delta^{1-2i}\int_0^1 g^{(i)}(\beta^2, R)h_{i,j}^{(2(m+i)-j+1))}(r^*, \theta)\gamma^j(R\delta)^{2(m+i)-j+1}dR$$

where $C^*_{i,j}$ is a constant. Since $r^* \in [0, \delta']$, lemma 15 implies $|h_{i,j}^{(2(m+i)-j+1))}(r^*, \theta)| \leq C_1$ for all $\theta \in [0, 2\pi]$. By lemma 18, $R^{2i}g^{(i)}(\beta^2, R) \leq C_2$. Because $2m - 2j + 1 \geq 0$, we have $R^{2m-2j+1} \leq 1$. Putting these estimates together we get

$$|I_{i,j}| \leq C^*_{i,j}C_1C_2\delta^{2m+2i-j+2-2i}|\gamma|^j \leq C|\gamma|\delta^{2m+1} \tag{4.32}$$

for some constant C independent of θ, δ, and γ.

After dropping the remainder terms in equation (4.30) and plugging the Taylor series expansions of the $h_{i,j}$ terms into equation (4.29) we get the following approximation of I_i

$$I_i^* = \delta^{1-2i}\int_0^1 g^{(i)}(\beta^2, R)\sum_{j=0}^{i} C_{i,j}\gamma^j \sum_{k=4i-2j}^{2(m+i)-j+1-a(j)} h_{i,j}^{(k)}(0, \theta)\frac{(R\delta)^k}{k!}dR$$

where we used the fact that $h_{i,j}(r, \theta) = O(r^{4i-2j})$. The only terms that depend on R look like $g^{(i)}(\beta^2, R)R^k$ where $k \geq 4i - 2j \geq 2i$. Hence, by lemma 18 these terms can be integrated and replaced with constants $R_{i,j,k}$ that are independent of θ, δ, and γ. After integration in R we thus have

$$I_i^* = \delta^{1-2i}\sum_{j=0}^{i} C_{i,j}\gamma^j \sum_{k=4i-2j}^{2(m+i)-j+1-a(j)} R_{i,j,k}h_{i,j}^{(k)}(0, \theta)\frac{(\delta)^k}{k!}$$

$$= \sum_{j=0}^{i} \sum_{k=4i-2j}^{2(m+i)-j+1-a(j)} C_{i,j,k}(\delta, \gamma)h_{i,j}^{(k)}(0, \theta)$$

for some constants $C_{i,j,k}(\delta, \gamma)$ that are independent of θ. By lemma 17, $h_{i,j}^{(k)}(0, \theta)$ is a trigonometric polynomial of degree at most k. Hence, for all $i \in \{0, \ldots, 2m\}$, I_i^* is also a trigonometric polynomial. It remains to determine the maximum degree of each I_i^*. Finding the maximum degree involves finding the largest upper limit over all nonzero k-sums. For a k-sum to be nonzero, the upper limit $2(m+i)-j+1-a(j)$ must be greater than or equal to the lower limit $4i - 2j$.

We consider two cases. First assume that $j = 0$. For the k-sum to be nonzero, we must have $2m + 2i + 1 - 4i = 2m - 2i + 1 \geq 0$. But since $2m - 2i + 1$ is odd we must have $2m - 2i + 1 > 0$. Rearranging we see that $2i < 2m + 1$ or $2i \leq 2m$. Plugging this into the upper limit of the sum gives $k \leq 2m + 2i + 1 \leq 2m + 2m + 1 = 4m + 1$. Thus the trigonometric polynomials corresponding to $j = 0$ have degree at most $4m + 1$ for all $i \in \{0, \ldots, 2m\}$. Next assume that $j > 0$ and hence $a(j) = 1$. In this case, we must have $2m + 2i - j - 4i + 2j = 2m - 2i + j \geq 0$. Rearranging we see that $2i - j \leq 2m$. Plugging this equation into the upper limit of the sum gives $k \leq 2m + 2m = 4m$. Thus the trigonometric polynomials corresponding to $j > 0$ have degree at most $4m$ for all $i \in \{0, \ldots, 2m\}$.

Thus, I_i^* is a trigonometric polynomial of degree at most $4m + 1$ for all $i \in \{0, \ldots, 2m\}$. Hence, we can approximate I with the trigonometric polynomial of degree at most $4m+1$ given by $\sum_{i=0}^{2m} I_i^*$. By equations (4.28), (4.31), and (4.32), the overall approximation error satisfies

$$\left| I - \sum_{i=0}^{2m} I_i^* \right| \leq C_1 \delta^{2m+3} + C_2 |\gamma| \delta^{2m+1}$$

for some constants C_1 and C_2 that are independent of θ, δ, and γ.

4.4 The Radial Integral Formula I : Derivation

In this section we consider the integral given by equation (4.15). More specifically, we derive the radial integral formula given in equation (4.43).

4.4.1 Helper Functions and a Variable Transformation

We start to integrate $I(\delta, \gamma)$, see equation (4.15), by expanding $f(r)$ into a Taylor series

$$f(r) = f(0) + f'(0)r + \cdots + \frac{f^{(i)}(0)}{i!}r^i + \cdots$$

and integrating term by term. We thus reduce to computing integrals such as

$$I_i(\delta, \gamma) = \int_{-\delta}^{\delta} \frac{|r|r^i g_i(r)}{(r^2 + (z(r) - \gamma)^2)^{1/2}} \zeta_\delta((r^2 + (z(r) - \gamma)^2)^{1/2}) dr$$

where $g_i(r)$ is a helper function to be determined. Unfortunately, this integral is still impossible to compute directly because of the dependence on $z(r)$. We thus seek a variable transformation that will simplify the integral. We define

$$y(r) = r\left(1 + \frac{z^2}{r^2} - \frac{2\gamma z}{r^2}\right)^{1/2} \tag{4.33}$$

and note that $y^2 = r^2 + z^2 - 2\gamma z$. Differentiating implicitly we see that

$$y_r(r) = \frac{r + z z_r - \gamma z_r}{y} \tag{4.34}$$

For sufficiently small δ, $y_r(r) > 0$ for all $r \in [-\delta, \delta]$ and $\gamma \in [-\delta, \delta]$. Thus $y(r)$ has a smooth inverse $r(y)$ with derivative $r_y(y) = \frac{1}{y_r(r(y))}$. Applying the substitution $y^2 = r^2 + z^2 - 2\gamma z$ we see that

$$I_i(\delta, \gamma) = \int_{-\delta}^{\delta} \frac{|r(y)|r_y(y)r(y)^i g_i(r(y))}{(y^2 + \gamma^2)^{1/2}} \zeta_\delta((y^2 + \gamma^2)^{1/2}) dy$$

Note that since $(y(\pm\delta))^2 + \gamma^2 = \delta^2 + (z(\pm\delta) - \gamma)^2 \geq \delta^2$ we can replace the limits of integration $y(\pm\delta)$ with $\pm\delta$. For the helper function $g_i(r)$, we choose a function close to the identity that simplifies the numerator. As a first guess we consider using

$$\bar{g}_i(r) = y_r(r) \left(\frac{y(r)}{r} \right)^{i+1}$$

If we plug in $\bar{g}_i(r)$ for $g_i(r)$, the numerator reduces to

$$|r(y)| r_y(y) y_r(r(y)) r(y)^i \left(\frac{y}{r(y)} \right)^i \left| \frac{y}{r(y)} \right| = |y| y^i$$

where we used the fact that $y(r)/r = |y(r)/r|$. We use the following formulas

$$\frac{y(r)}{r} = \left(1 + \frac{z^2}{r^2} - \frac{2\gamma z}{r^2} \right)^{1/2}, \qquad y_r(r) \frac{y(r)}{r} = \left(1 + \frac{z z_r}{r} - \gamma \frac{z_r}{r} \right) \tag{4.35}$$

to compute the limits

$$\lim_{r \to 0} \frac{y(r)}{r} = \alpha, \qquad \lim_{r \to 0} y_r(r) = \alpha$$

where $\alpha = (1 - \gamma z_{rr}(0))^{1/2}$. Since we want $g_i(r)$ to be close to the identity, we define

$$g_i(r) = \frac{y_r(r)}{\alpha} \left(\frac{y(r)}{\alpha r} \right)^{i+1} \tag{4.36}$$

and note that for each $i \geq 0$ we have $g_i(r) \in C^\infty([-\delta, \delta])$ and $g_i(r) = 1 + O(\gamma r) + O(r^2)$. Returning to $I_i(\delta, \gamma)$ we see that

$$I_i(\delta, \gamma) = \frac{1}{\alpha^{i+2}} \int_{-\delta}^{\delta} \frac{|y| y^i}{(y^2 + \gamma^2)^{1/2}} \zeta_\delta((y^2 + \gamma^2)^{1/2}) dy$$

and note that $I_i(\delta, \gamma) = 0$ for i odd by symmetry. Next we remove the dependence on δ by setting $u = y/\delta$. This gives

$$I_i(\delta, \gamma) = \frac{\delta^{i+1}}{\alpha^{i+2}} \int_{-1}^{1} \frac{|u| u^i}{(u^2 + \beta^2)^{1/2}} \zeta((u^2 + \beta^2)^{1/2}) du$$

where $\beta = |\gamma|/\delta$. We denote the remaining radial integral by $\Lambda_i(\beta)$ and consider its exact computation later. We thus arrive at the following integration formula which will be foundational for our radial integration method.

$$I_i(\delta, \gamma) = \frac{\delta^{i+1}}{\alpha^{i+2}} \Lambda_i(\beta) \tag{4.37}$$

4.4.2 The Remainder Recurrence

The helper function $g_i(r)$ allows us to change a complex integral into one that can be integrated exactly. However, because $g_i(r) = 1 + O(\gamma r) + O(r^2)$ is not exactly the identity, we also need to consider the remainder terms. The following recurrence relation enables a systematic approach. We define

$$f_0(r) = f(r) \tag{4.38}$$

and for $n \geq 0$

$$f_{n+1}(r) = f_n(r) - f_n^{(n)}(0) \frac{r^n}{n!} g_n(r) \tag{4.39}$$

A key property of the recurrence is that $f_{n+1}(r) = O(r^{n+1})$ for all $n \geq 0$. This fact is a corollary of the following lemma.

Lemma 19. *For $n \geq 0$ we have $f_{n+1}^{(i)}(0) = 0$ for all $i \leq n$.*

Proof. Define $h_n = (r^n/n!) g_n(r)$ and note that for $i < n$

$$h_n^{(i)}(0) = 0 \tag{4.40}$$

We use induction on n. Let $n = 0$. Since $g_0(0) = 1$,

$$f_1^{(0)}(0) = f_1(0) = f(0) - f(0) g_0(0) = 0$$

For the inductive step, assume $n > 0$. If $i < n$, then

$$f_{n+1}^{(i)}(0) = f_n^{(i)}(0) - f_n^{(n)}(0) h_n^{(i)}(0) = 0$$

by the inductive hypothesis and equation (4.40). Next assume that $i = n$. Using the fact that $h_n^{(n)}(0) = g_n(0) = 1$ we see that

$$f_{n+1}^{(n)}(0) = f_n^{(n)}(0) - f_n^{(n)}(0)g_n(0) = 0$$

□

The recurrence defined by equations (4.38) and (4.39) can be solved for an explicit formula. For $n \geq 0$, we have that

$$f_{n+1}(r) = f(r) - \sum_{i=0}^{n} \frac{f_i^{(i)}(0)}{i!} r^i g_i(r)$$

Rearranging terms we see that

$$f(r) = \sum_{i=0}^{n} \frac{f_i^{(i)}(0)}{i!} r^i g_i(r) + f_{n+1}(r) \tag{4.41}$$

Since $f_{n+1}(r) = O(r^{n+1})$ we note that

$$\int_{-\delta}^{\delta} \frac{|r| f_{n+1}(r)}{(r^2 + (z(r) - \gamma)^2)^{1/2}} \zeta_\delta((r^2 + (z(r) - \gamma)^2)^{1/2}) dr = O(\delta^{n+2}) \tag{4.42}$$

Plugging (4.41) into (4.15) and using (4.37) and (4.42) we have that

$$I(\delta, \gamma) = \sum_{i=0}^{n} \frac{f_i^{(i)}(0)}{i!} \frac{\delta^{i+1}}{\alpha^{i+2}} \Lambda_i(\beta) + O(\delta^{n+2})$$

By using the fact that $\Lambda_i(\beta) = 0$ for i odd, this formula can be sharpened to the *radial integral formula*

$$I(\delta, \gamma) = \sum_{k=0}^{m} \frac{f_{2k}^{(2k)}(0)}{(2k)!} \frac{\delta^{2k+1}}{\alpha^{2k+2}} \Lambda_{2k}(\beta) + O(\delta^{2m+3}) \tag{4.43}$$

4.5 The Radial Integral Formula II : Standard Radial Integrals

In this section we consider the computation of the integrals defined for all $i \geq 0$ as

$$\Lambda_i(\beta) = \int_{-1}^{1} \frac{|u|u^i}{(u^2+\beta^2)^{1/2}} \zeta((u^2+\beta^2)^{1/2}) du \tag{4.44}$$

We assume throughout that $\zeta(r) = 1$ for $r \in [-\eta, \eta]$ and that that $\beta \in [0, \eta]$.

In our work, we make use of certain precomputed integrals involving ζ, called the *standard radial integrals*, to assist in evaluating the $\Lambda_i(\beta)$ terms in constant time. For a non-negative integer i we define

$$\zeta_i = \int_{-1}^{1} x^i \zeta(x) dx \tag{4.45}$$

By symmetry, $\zeta_i = 0$ for i odd. For i even, the values of ζ_i can be precomputed using the trapezoid rule. Because the integrand is smooth and there is no boundary, ζ_i can be evaluated to machine precision with only a few hundred quadrature points.

4.5.1 Simple Cases

We start with some simple cases. For i odd, $\Lambda_i(\beta) = 0$. For i even, we have by symmetry that

$$\Lambda_i(\beta) = 2\int_{0}^{1} \frac{u^{i+1}}{(u^2+\beta^2)^{1/2}} \zeta((u^2+\beta^2)^{1/2}) du$$

We start with the $i = 0$ case

$$\Lambda_0(\beta) = 2\int_{0}^{1} \frac{u}{(u^2+\beta^2)^{1/2}} \zeta((u^2+\beta^2)^{1/2}) du$$

By letting $v^2 = u^2 + \beta^2$ we see that $vdv = udu$ and thus

$$\Lambda_0(\beta) = 2\int_{0}^{1} \zeta(v) dv - 2\int_{0}^{\beta} \zeta(v) dv$$

Since $\beta \leq \eta$, we have that

$$\Lambda_0(\beta) = \int_{-1}^{1} \zeta(v)dv - 2\int_0^{\beta} dv = \zeta_0 - 2\beta \tag{4.46}$$

Note that we made critical use of the local flatness of ζ to pull the β out of the integral. Next consider the $i = 2$ case

$$\Lambda_2(\beta) = 2\int_0^1 \frac{u^3}{(u^2+\beta^2)^{1/2}}\zeta((u^2+\beta^2)^{1/2})du$$

We let $v^2 = u^2 + \beta^2$ again and compute

$$\Lambda_2(\beta) = 2\int_0^1 (v^2-\beta^2)\zeta(v)dv - 2\int_0^{\beta}(v^2-\beta^2)dv = \zeta_2 - \beta^2\zeta_0 + 4\beta^3/3 \tag{4.47}$$

4.5.2 General Formula

Using the substitution $v^2 = u^2 = \beta^2$ and the binomial theorem, a general formula can be derived for all even i.

Lemma 20. *Let $\beta \in [0, \eta]$, and k be a non-negative integer. Then*

$$\Lambda_{2k}(\beta) = \sum_{i=0}^{k}(-\beta^2)^{k-i}\frac{k!}{i!(k-i)!}\zeta_{2i} - 2\beta^{2k+1}\sum_{i=0}^{k}\frac{(-1)^{k-i}}{2i+1}\frac{k!}{i!(k-i)!} \tag{4.48}$$

Proof. We wish to compute

$$I = \Lambda_{2k}(\beta) = 2\int_0^1 \frac{u^{2k+1}}{(u^2+\beta^2)^{(1/2)}}\zeta((u^2+\beta^2)^{(1/2)})du$$

We set $v^2 = u^2 + \beta^2$ and substitute v for u to get

$$I = 2\int_0^1 (v^2-\beta^2)^k\zeta(v)dv - 2\int_0^{\beta}(v^2-\beta^2)^k dv$$

Using the binomial theorem we compute

$$I = 2\sum_{i=0}^{k}(-\beta^2)^{k-i}\frac{k!}{i!(k-i)!}\int_0^1 v^{2i}\zeta(v)dv - 2\sum_{i=0}^{k}(-\beta^2)^{k-i}\frac{k!}{i!(k-i)!}\int_0^\beta v^{2i}dv$$

After integrating and noting that $(-\beta^2)^{k-i}\beta^{2i+1} = (-1)^{k-i}\beta^{2k+1}$ we compute

$$I = \sum_{i=0}^{k}(-\beta^2)^{k-i}\frac{k!}{i!(k-i)!}\zeta_{2i} - 2\beta^{2k+1}\sum_{i=0}^{k}\frac{(-1)^{k-i}}{2i+1}\frac{k!}{i!(k-i)!}$$

□

Note that for $\beta = 0$ the result of lemma 20 is simply

$$\Lambda_{2k}(0) = \zeta_{2k} \tag{4.49}$$

For our numerical testing we will require formulas for $k \in \{0,1,2,3\}$. For $k \in \{0,1\}$ the formulas appear in equations (4.46) and (4.47). For convenience, we present the formulas for the $k \in \{2,3\}$ cases as well.

$$\Lambda_4(\beta) = \zeta_4 - 2\beta^2\zeta_2 + \beta^4\zeta_0 - 16\beta^5/15 \tag{4.50}$$

$$\Lambda_6(\beta) = \zeta_6 - 3\beta^2\zeta_4 + 3\beta^4\zeta_2 - \beta^6\zeta_0 + 32\beta^7/35 \tag{4.51}$$

4.6 The Radial Integral Formula III : Estimation Algorithms

For simplicity, we assume throughout this section that $\gamma = O(\delta^2)$ and leave the more general case for future research.

The integral formula given in equation (4.43) will be our principal tool for approximating the radial part of a localized single layer potential. To use the formula, many terms will have to be estimated given regularly spaced samples of the functions f, z, and z_r (see section 4.6.3 for input assumptions). The goal of this section is to describe an estimation procedure for the necessary terms such that the additional error introduced matches the truncation error of $O(\delta^{2m+3})$ in order.

4.6.1 Estimating the Recursive Function Derivatives

To use equation (4.43), we will need to estimate $f_i^{(i)}(0)$ for $i \in \{0, \ldots, 2m\}$ numerically. The following lemma gives a recurrence for the $f_i^{(i)}(0)$ terms.

Lemma 21. *For all $i \geq 0$ we have*

$$f_i^{(i)}(0) = f^{(i)}(0) - \sum_{j=0}^{i-1} \frac{i!}{j!(i-j)!} f_j^{(j)}(0) g_j^{(i-j)}(0) \tag{4.52}$$

Proof. We need to differentiate the explicit formula

$$f_i(r) = f(r) - \sum_{j=0}^{i-1} \frac{f_j^{(j)}(0)}{j!} r^j g_j(r)$$

i times and plug in $r = 0$. Let

$$h(r) = \sum_{j=0}^{i-1} \frac{f_j^{(j)}(0)}{j!} r^j g_j(r)$$

Using the Leibniz rule for products we compute

$$h^{(i)}(r) = \sum_{j=0}^{i-1} \frac{f_j^{(j)}(0)}{j!} \sum_{k=0}^{j} \frac{i!}{k!(i-k)!} \frac{j!}{(j-k)!} r^{j-k} g_j^{(i-k)}(r)$$

Upon plugging in $r = 0$ all terms except the $k = j$ term of the second sum are zero. Thus

$$h^{(i)}(0) = \sum_{j=0}^{i-1} \frac{f_j^{(j)}(0)}{j!} \frac{i!}{j!(i-j)!} \frac{j!}{(j-j)!} r^{j-j} g_j^{(i-j)}(0) = \sum_{j=0}^{i-1} \frac{i!}{j!(i-j)!} f_j^{(j)}(0) g_j^{(i-j)}(0)$$

□

To emphasize the Taylor series coefficients, we sometimes rewrite equation (4.52) as

$$\frac{f_i^{(i)}(0)}{i!} = \frac{f^{(i)}(0)}{i!} - \sum_{j=0}^{i-1} \frac{f_j^{(j)}(0)}{j!} \frac{g_j^{(i-j)}(0)}{(i-j)!} \tag{4.53}$$

We next prove two approximation lemmas. We will use the function $a : \mathbb{Z} \to \mathbb{Z}$ defined as

$$a(i) = i + (i \mod 2)$$

Lemma 22. *Suppose that for all $i \in \{0, \ldots, 2m\}$ we have approximations of $f^{(i)}(0)$, which we call $\bar{f}^{(i)}(0)$, that satisfy*

$$\bar{f}^{(i)}(0) = f^{(i)}(0) + O(\delta^{2m+2-a(i)}) \tag{4.54}$$

and for all $i \in \{1, \ldots, 2m\}$ and $j \in \{0, \ldots, i-1\}$ we have approximations of $g_j^{(i-j)}(0)$, which we call $\bar{g}_j^{(i-j)}(0)$, that satisfy

$$\bar{g}_j^{(i-j)}(0) = g_j^{(i-j)}(0) + O(\delta^{2m+2-a(i-j)}) \tag{4.55}$$

Then if we compute the approximation $\bar{f}_i^{(i)}(0)$ for all $0 \leq i \leq 2m$ using the equation

$$\frac{\bar{f}_i^{(i)}(0)}{i!} = \frac{\bar{f}^{(i)}(0)}{i!} - \sum_{j=0}^{i-1} \frac{\bar{f}_j^{(j)}(0)}{j!} \frac{\bar{g}_j^{(i-j)}(0)}{(i-j)!} \tag{4.56}$$

we have that

$$\bar{f}_i^{(i)}(0) = f_i^{(i)}(0) + O(\delta^{2m+2-a(i)}) \tag{4.57}$$

for all $0 \leq i \leq 2m$.

Proof. We use induction on i. By assumption $\bar{f}_0^{(0)}(0) = \bar{f}^{(0)}(0) = f^{(0)}(0) + O(\delta^{2m+2})$. For the inductive step suppose that $\bar{f}_j^{(j)}(0) = f_j^{(j)}(0) + O(\delta^{2m+2-a(j)})$ for all $0 \leq j < i$. Plugging what we know into equation (4.56) gives

$$\frac{\bar{f}_i^{(i)}(0)}{i!} = \left(\frac{f^{(i)}(0)}{i!} + O(\delta^{2m+2-a(i)}) \right)$$

$$-\sum_{j=0}^{i-1}\left(\frac{f_j^{(j)}(0)}{j!}+O(\delta^{2m+2-a(j)})\right)\left(\frac{g_j^{(i-j)}(0)}{(i-j)!}+O(\delta^{2m+2-a(i-j)})\right)$$

We note that for all $0 \leq j \leq i-1$ we have that $a(j) \leq a(i)$ and $a(i-j) \leq a(i)$. Thus $(2m+2-a(j)) \geq (2m+2-a(i))$ and $(2m+2-a(i-j)) \geq (2m+2-a(i))$. After simplifying and using equation (4.53) we see that $\bar{f}_i^{(i)}(0) = f_i^{(i)}(0)+O(\delta^{2m+2-a(i)})$. □

Lemma 23. *Suppose that for all $0 \leq k \leq m$ we have that $\bar{f}_{2k}^{(2k)}(0)$ is approximated as in lemma 22. Then we have*

$$I(\delta,\gamma) = \sum_{k=0}^{m} \frac{\bar{f}_{2k}^{(2k)}(0)}{(2k)!}\frac{\delta^{2k+1}}{\alpha^{2k+2}}\Lambda_{2k}(\beta) + O(\delta^{2m+3}) \tag{4.58}$$

Proof. Because $a(i) = i$ for i even, equation (4.57) says that $\bar{f}_{2k}^{(2k)}(0) = f_{2k}^{(2k)}(0) + O(\delta^{2m+2-2k})$ for all $0 \leq k \leq m$. Plugging $\bar{f}_{2k}^{(2k)}(0)$ into equation (4.58) gives

$$I(\delta,\gamma) = \sum_{k=0}^{m} \frac{f_{2k}^{(2k)}(0) + O(\delta^{2m+2-2k})}{(2k)!}\frac{\delta^{2k+1}}{\alpha^{2k+2}}\Lambda_{2k}(\beta) + O(\delta^{2m+3})$$

The result follows by noting that $2m+2-2k+2k+1 = 2m+3$ and using equation (4.43). □

Together, lemmas 22 and 23 show that if we compute $\bar{f}^{(i)}(0)$ and $\bar{g}_j^{(i-j)}(0)$ according to equations (4.54) and (4.55), use equation (4.56) to compute the $\bar{f}_i^{(i)}(0)$ terms, and finally use equation (4.58) to estimate $I(\delta,\gamma)$, then we obtain an overall $O(\delta^{2m+3})$ approximation error.

4.6.2 Centered Finite Differences

It is a well known fact [6] that if the $(2m+1)$-point centered finite-difference formula with grid spacing $O(\delta)$ is used to compute the i^{th} derivative at $r = 0$ of a smooth function $s(r)$ for $i \in \{1,\ldots,2m\}$, then the truncation error is $O(\delta^{2m+2-a(i)})$. In

addition, to compute the i^{th} derivative we need to divide the weighted samples of $s(r)$ by $O(\delta^i)$ which introduces an additional error determined by the accuracy of the samples of $s(r)$. The following lemma gives the result we need for estimating derivatives.

Lemma 24. *Let $m > 0$ and define $h = \delta/m$, $r_l = -\delta + hl$, and assume samples of a smooth function $s(r)$ that satisfy $\bar{s}(r_l) = s(r_l) + O(\delta^{2m+2})$ for all $l \in \{0, \ldots, 2m\}$. Further, suppose that the $(2m+1)$-point centered finite difference weights for approximating the i^{th} derivative at $r = 0$ are given by $\{w_l^{m,i}\}_{l=0}^{2m}$. Then for all $i \in \{1, \ldots, 2m\}$ we have*

$$\sum_{l=0}^{2m} w_l^{m,i} h^{-i} \bar{s}(r_l) = s^{(i)}(0) + O(\delta^{2m+2-a(i)}) \tag{4.59}$$

Proof. We start with the standard truncation error estimate

$$\sum_{l=0}^{2m} w_l^{m,i} h^{-i} s(r_l) = s^{(i)}(0) + O(\delta^{2m+2-a(i)}) \tag{4.60}$$

Next we plug what we know about $\bar{s}(r_l)$ into the left hand side of equation (4.59) and compute

$$\sum_{l=0}^{2m} w_l^{m,i} h^{-i} \bar{s}(r_l) = \sum_{l=0}^{2m} w_l^{m,i} h^{-i} \left(s(r_l) + O(\delta^{2m+2}) \right) = s^{(i)}(0) + O(\delta^{2m+2-a(i)})$$

where we used equation (4.60) and the fact that $2m + 2 - i \geq 2m + 2 - a(i)$ □

Although tables of the weights $\{w_l^{m,i}\}_{l=0}^{2m}$ are easy to find in the literature for $m \in \{1, 2\}$, we require the weights for $m = 3$ as well. A simple method for determining the weights $\{w_l^{m,i}\}_{l=0}^{2m}$ for an arbitrary m is given in [5]. Using a rational arithmetic implementation of the method, we compute the weight tables for $m = 3$. For convenience, we give the weight tables for $m \in \{1, 2, 3\}$, which are needed for our numerical testing, in appendix D.

4.6.3 Input Assumptions

Assume as input an estimated value of γ that satisfies $\bar{\gamma} = \gamma + O(\delta^{2m+3})$. Further assume as inputs the functions $f(r)$, $z(r)$, and $z_r(r)$ on a regular grid with $2m+1$ points centered at the origin. More specifically, define $h = \delta/m$ and $r_l = -\delta + hl$ as in lemma 24 and assume as inputs the values $\{\bar{f}(r_l)\}_0^{2m}$, $\{\bar{z}(r_l)\}_0^{2m}$, and $\{\bar{z_r}(r_l)\}_0^{2m}$ satisfying

$$\bar{f}(r_l) = f(r_l) + O(\delta^{2m+2}), \quad \bar{z}(r_l) = z(r_l) + O(\delta^{2m+2}), \quad \bar{z_r}(r_l) = z_r(r_l) + O(\delta^{2m+1}) \tag{4.61}$$

for all $l \in \{0, \ldots, 2m\}$. Note that we could compute the $\bar{z_r}(r_l)$ terms to the needed order by using $(2m+1)$-point centered finite differences on $\bar{z}$ samples provided that we had $\bar{z}$ sampled on a grid with $4m+1$ points. We avoid this additional complexity and assume the set $\{\bar{z_r}(r_l)\}_0^{2m}$ as input. This assumption seems reasonable given our intended application of these methods to implicitly defined surfaces for which the gradient of the level set function is known.

4.6.4 Further Estimations

To use the results of section 4.6.1 we see by equation (4.54) that we need to estimate $f^{(i)}(0)$ with an error of $O(\delta^{2m+2-a(i)})$ for all $0 \leq i \leq 2m$. Using the input assumptions displayed in equation (4.61) and the result of lemma 24, we can estimate $f^{(i)}(0)$ to the desired order by setting

$$\bar{f}^{(0)}(0) = \bar{f}(r_m) \tag{4.62}$$

and for all $i \in \{1, \ldots, 2m\}$

$$\bar{f}^{(i)}(0) = \sum_{l=0}^{2m} w_l^{m,i} h^{-i} \bar{f}(r_l) \tag{4.63}$$

Next, we consider the estimation of $\alpha = (1 - \gamma z_{rr}(0))^{1/2}$. First we let

$$\overline{z_{rr}}(0) = \sum_{l=0}^{2m} w_l^{m,2} h^{-2} \bar{z}(r_l) \tag{4.64}$$

and note that $\overline{z_{rr}}(0) = z_{rr}(0) + O(\delta^{2m})$. Set

$$\bar{\alpha} = (1 - \bar{\gamma}\overline{z_{rr}}(0))^{1/2} \tag{4.65}$$

Plugging in our estimates gives

$$\bar{\alpha} = (1 - (\gamma + O(\delta^{2m+3}))(z_{rr}(0) + O(\delta^{2m})))^{1/2}$$

We note that $\bar{\alpha} = \alpha + O(\delta^{2m+2})$ where we used the fact that $\gamma = O(\delta^2)$. Furthermore, using a simple Taylor argument one can show that for all $i > 0$ we have

$$\frac{1}{\bar{\alpha}^i} = \frac{1}{\alpha^i} + O(\delta^{2m+2}) \tag{4.66}$$

We next give estimations of the $g_j^{(i-j)}(0)$ terms that satisfy equation (4.55). First we generate approximate samples of the functions $g_0(r) = y_r(r)(y(r)/\alpha^2 r)$ and $g(r) = y(r)/\alpha r$ using equations (4.35) and (4.65). More specifically, set

$$\bar{g_0}(0) = 1, \qquad \bar{g}(0) = 1$$

and for all $l \in \{0, \ldots, 2m\}$ such that $l \neq m$ we set

$$\bar{g_0}(r_l) = \frac{1}{\bar{\alpha}^2}\left(1 + \frac{\bar{z}(r_l)\bar{z_r}(r_l)}{r_l} - \frac{\bar{\gamma}\bar{z_r}(r_l)}{r_l}\right), \quad \bar{g}(r_l) = \frac{1}{\bar{\alpha}}\left(1 + \frac{\bar{z}(r_l)^2}{r_l^2} - \frac{2\bar{\gamma}\bar{z}(r_l)}{r_l^2}\right)^{1/2} \tag{4.67}$$

Using the facts that

$$\bar{z}(r_l) = z(r_l) + O(\delta^{2m+2}), \quad \bar{z_r}(r_l) = z_r(r_l) + O(\delta^{2m+1}), \quad \bar{\gamma} = \gamma + O(\delta^{2m+3})$$

as well as

$$z(r_l) = O(\delta^2), \quad z_r(r_l) = O(\delta), \quad \gamma = O(\delta^2), \quad r_l = O(\delta)$$

we see that

$$\frac{\bar{z}(r_l)\bar{z_r}(r_l)}{r_l} = \frac{z(r_l)z_r(r_l)}{r_l} + O(\delta^{2m+2}), \quad \frac{\bar{\gamma}\bar{z_r}(r_l)}{r_l} = \frac{\gamma z_r(r_l)}{r_l} + O(\delta^{2m+2})$$

and

$$\frac{\bar{z}(r_l)^2}{r_l^2} = \frac{z(r_l)^2}{r_l^2} + O(\delta^{2m+2}), \quad \frac{2\bar{\gamma}\bar{z}(r_l)}{r_l^2} = \frac{2\gamma z(r_l)}{r_l^2} + O(\delta^{2m+2})$$

Combining these facts with equation (4.66) shows that for all $l \in \{0, \ldots, 2m\}$ we have

$$\bar{g_0}(r_l) = g_0(r_l) + O(\delta^{2m+2}), \quad \bar{g}(r_l) = g(r_l) + O(\delta^{2m+2}) \tag{4.68}$$

Next we define for all $i \in \{1, \ldots, 2m-1\}$ and $l \in \{0, \ldots, 2m\}$

$$\bar{g_i}(r_l) = \overline{g_{i-1}}(r_l)\bar{g}(r_l) \tag{4.69}$$

Using a simple induction argument as well equation (4.68), one can show that for all $i \in \{1, \ldots, 2m-1\}$ and for all $l \in \{0, \ldots, 2m\}$ we have

$$\bar{g_i}(r_l) = g_i(r_l) + O(\delta^{2m+2}) \tag{4.70}$$

Finally, as before with $f(r)$, we estimate the terms $g_j^{(i-j)}(0)$ for all $i \in \{1, \ldots, 2m\}$ and for all $j \in \{0, \ldots, i-1\}$ by using our estimated samples and $(2m+1)$-point centered finite differences. More specifically, set for all $i \in \{1, \ldots, 2m\}$ and for all $j \in \{0, \ldots, i-1\}$

$$\bar{g_j}^{(i-j)}(0) = \sum_{l=0}^{2m} w_l^{m,i-j} h^{-(i-j)} \bar{g_i}(r_l) \tag{4.71}$$

and note that by lemma 24 we have $\bar{g_j}^{(i-j)}(0) = g_j^{(i-j)}(0) + O(\delta^{2m+2-a(i-j)})$.

Let $m \geq 0$ be a given parameter. In practice, the value of β will be estimated and thus $\Lambda_{2k}(\beta)$ will be as well. By considering equation (4.58) we see that in order to limit the overall error in approximating $I(\delta, \gamma)$ to $O(\delta^{2m+3})$ we will need estimated values that satisfy

$$\Lambda_{2k}(\bar{\beta}) = \Lambda_{2k}(\beta) + O(\delta^{2m+2-2k}) \tag{4.72}$$

for all $k \in \{0, \ldots, m\}$. Define $\bar{\beta} = |\bar{\gamma}|/\delta$ and note that $\bar{\beta} = \beta + O(\delta^{2m+2})$ where $\beta = |\gamma|/\delta$ because $\bar{\gamma} = \gamma + O(\delta^{2m+3})$. Finally, looking at equation (4.48) we see that $\Lambda_{2k}(\bar{\beta}) = \Lambda_{2k}(\beta) + O(\delta^{2m+2})$ for all $k \geq 0$ and thus equation (4.72) is satisfied.

4.6.5 A Complete Estimation Algorithm

Let $m \geq 0$ and $\delta > 0$ be given parameters. In this section we give a complete algorithm for estimating $I(\delta, \gamma)$ with an overall error of $O(\delta^{2m+3})$. We assume that for all $k \in \{0, \ldots, m\}$ the values of ζ_{2k}, see equation (4.45), have been precomputed to machine precision and stored in a lookup table. We assume that the inputs specified in section 4.6.3 are given. More specifically, assume $\bar{\gamma}$ is given as well as the sets $\{\bar{f}(r_l)\}_0^{2m}$, $\{\bar{z}(r_l)\}_0^{2m}$, and $\{\bar{z}_r(r_l)\}_0^{2m}$ that satisfy equation (4.61). Further assume the sets $\{w_l^{m,i}\}_{l=0}^{2m}$ contain the $(2m+1)$-point centered finite difference weights. Let $h = \delta/m$ and $r_l = -\delta + hl$ for all $l \in \{0, \ldots, 2m\}$. The following is the step by step procedure.

1. Set $\bar{\beta} = |\bar{\gamma}|/\delta$ and for all $k \in \{0, \ldots, m\}$, use equation (4.48) to compute $\Lambda_{2k}(\bar{\beta})$.

2. Set $\overline{z_{rr}}(0) = \sum_{l=0}^{2m} w_l^{m,2} \bar{z}(r_l) h^{-2}$ and $\bar{\alpha} = \sqrt{1 - \bar{\gamma}\overline{z_{rr}}(0)}$.

3. Set $\bar{g}_0(0) = 1$ and $\bar{g}(0) = 1$. For all $l \in \{0, \ldots, 2m\}$ such that $l \neq m$ set

$$\bar{g}_0(r_l) = \frac{1}{\bar{\alpha}^2}\left(1 + \bar{z}(r_l)\bar{z}_r(r_l)/r_l - \bar{\gamma}\bar{z}_r/r_l\right)$$

and

$$\bar{g}(r_l) = \frac{1}{\bar{\alpha}}\sqrt{1 + \bar{z}^2(r_l)/r_l^2 - 2\bar{\gamma}\bar{z}(r_l)/r_l^2}$$

4. For all $i \in \{1, \ldots, 2m-1\}$ and $l \in \{0, \ldots, 2m\}$ set $\bar{g}_i(r_l) = \overline{g_{i-1}}(r_l)\bar{g}(r_l)$.

5. For all $i \in \{0, \ldots, 2m\}$ set

$$\bar{f}^{(i)}(0) = \sum_{l=0}^{2m} w_l^{m,i} \bar{f}(r_l) h^{-i}$$

6. For all $i \in \{1, \ldots, 2m\}$ and $j \in \{0, \ldots, i-1\}$ set

$$\bar{g_j}^{(i-j)} = \sum_{l=0}^{2m} w_l^{m,i-j} \bar{g}_j(r_l) h^{-(i-j)}$$

7. For all $i \in \{0, \ldots, 2m\}$ set

$$\frac{\bar{f_i}^{(i)}(0)}{i!} = \frac{\bar{f}^{(i)}(0)}{i!} - \sum_{j=0}^{i-1} \frac{\bar{f_j}^{(j)}(0)}{j!} \frac{\bar{g_j}^{(i-j)}(0)}{(i-j)!}$$

8. Set

$$\bar{I}(\delta, \bar{\gamma}) = \sum_{k=0}^{m} \frac{\bar{f}_{2k}^{(2k)}(0)}{(2k)!} \frac{\delta^{2k+1}}{\bar{\alpha}^{2k+2}} \Lambda_{2k}(\bar{\beta})$$

By the theory developed in this section, we have that

$$\bar{I}(\delta, \bar{\gamma}) = I(\delta, \gamma) + O(\delta^{2m+3}) \tag{4.73}$$

We next give a simple optimization of the procedure. If we pull a δ out of the sum in the last step we are left with terms like $\bar{f}_{2k}^{(2k)}(0)\delta^{2k}$. If we unfold the recursion we see that the i^{th} derivatives are always paired up with a δ^i term. Thus, the δ^i terms can be cancelled with the h^{-i} terms that are used throughout to approximate the derivatives using finite differences. Hence, instead of using $h = \delta/m$ we can use $h = 1/m$ for the derivative computations and omit the δ^{2k} terms in the formula for the last step.

4.7 Numerical Results I : Basic Verifications

The numerical tests of this section involve computing a localized single layer potential, see equation (4.2), with unit density ($\mu = 1$) at the evaluation point $x = (a, 0, 0)$ of an oblate ellipsoid which is the zero-set of the function

$$\phi(x) = \frac{x_1^2 + x_2^2}{a^2} + x_3^2 = 1 \tag{4.74}$$

for some parameter $a > 0$. Explicit formulas for the height function $Z(s,t)$ and its derivatives are given by

$$Z(s,t) = -a + a(1 - s^2/a^2 - t^2)^{1/2} \tag{4.75}$$

$$Z_s(s,t) = \frac{-s}{a(1 - s^2/a^2 - t^2)^{1/2}}, \qquad Z_t(s,t) = \frac{-at}{(1 - s^2/a^2 - t^2)^{1/2}} \tag{4.76}$$

Note further that

$$Z_{ss}(0,0) = -1/a, \qquad Z_{st}(0,0) = 0, \qquad Z_{tt}(0,0) = -a$$

so the principal curvatures are $\kappa_1 = -1/a$ and $\kappa_2 = -a$. In this section, we use $a = 5$ for our numerical testing.

4.7.1 Angular Integral Only

In this section we verify the convergence rate predicted by corollary 14 for computing the integral $\int_0^\pi B(\theta, \delta, \gamma) d\theta$. For a given $m \geq 0$ we use $h = \pi/(2m+1)$ and expect to see a convergence rate of $O(\delta^{2m+3}) + O(|\gamma|\delta^{2m+1})$. We use the locally flat cutoff function given by equation (A.1) with $\eta = 1/4$. Our test surface is the oblate ellipsoid given by equation (4.74) with parameter $a = 5$. In all cases, we compute the radial integrals to machine precision using the techniques given in appendix C. Since the radial integration is *exact*, the only errors in our tests are from the angular integral quadrature. To compute the angular error, we compare our approximate result with

the *exact* angular integral computed by setting the angular quadrature spacing to $h^* = \pi/25$.

The results for the singular case ($\gamma = 0$) are shown in table 4.1. We expect a convergence rate of $O(\delta^{2m+3})$. The results for the small distance nearly singular

Table 4.1: Angular Integral Test : $\gamma = 0$

δ	m	abs error	order	m	abs error	order	m	abs error	order
0.1	1	$1.34 \cdot 10^{-5}$		2	$1.25 \cdot 10^{-7}$		3	$1.00 \cdot 10^{-9}$	
0.05	1	$4.14 \cdot 10^{-7}$	5.02	2	$1.05 \cdot 10^{-9}$	6.89	3	$2.41 \cdot 10^{-12}$	8.70
0.025	1	$1.28 \cdot 10^{-8}$	5.01	2	$8.35 \cdot 10^{-12}$	6.98	3	$4.96 \cdot 10^{-15}$	8.93
0.0125	1	$4.01 \cdot 10^{-10}$	5.00	2	$6.55 \cdot 10^{-14}$	6.99	3		

case where the point is first outside the surface ($\gamma = \delta^4$) and then inside the surface ($\gamma = -\delta^4$) are shown in tables 4.2 and 4.3. We expect a convergence rate of $O(\delta^{2m+3})$ because $|\gamma| = O(\delta^2)$. The results for the medium distance nearly singular case where

Table 4.2: Angular Integral Test : $\gamma = \delta^4$

δ	m	abs error	order	m	abs error	order	m	abs error	order
0.1	1	$1.37 \cdot 10^{-5}$		2	$1.26 \cdot 10^{-7}$		3	$1.01 \cdot 10^{-9}$	
0.05	1	$4.16 \cdot 10^{-7}$	5.04	2	$1.06 \cdot 10^{-9}$	6.90	3	$2.42 \cdot 10^{-12}$	8.70
0.025	1	$1.29 \cdot 10^{-8}$	5.01	2	$8.36 \cdot 10^{-12}$	6.98	3	$4.96 \cdot 10^{-15}$	8.93
0.0125	1	$4.01 \cdot 10^{-10}$	5.00	2	$6.55 \cdot 10^{-14}$	7.00	3		

the point is first outside the surface ($\gamma = \delta^2$) and then inside the surface ($\gamma = -\delta^2$) are shown in tables 4.4 and 4.5. We expect a convergence rate of $O(\delta^{2m+3})$ because $|\gamma| = O(\delta^2)$. Finally, we test the large distance nearly singular case where the point is first outside the surface ($\gamma = \delta/6$) and then inside the surface ($\gamma = -\delta/4$). The results are shown in tables 4.6 and 4.7. Since $|\gamma| = O(\delta)$, we expect a convergence rate of $O(\delta^{2m+2})$.

Table 4.3: Angular Integral Test : $\gamma = -\delta^4$

δ	m	abs error	order	m	abs error	order	m	abs error	order
0.1	1	$1.31 \cdot 10^{-5}$		2	$1.23 \cdot 10^{-7}$		3	$9.97 \cdot 10^{-10}$	
0.05	1	$4.11 \cdot 10^{-7}$	4.99	2	$1.05 \cdot 10^{-9}$	6.88	3	$2.41 \cdot 10^{-12}$	8.69
0.025	1	$1.28 \cdot 10^{-8}$	5.00	2	$8.35 \cdot 10^{-12}$	6.97	3	$4.95 \cdot 10^{-15}$	8.93
0.0125	1	$4.01 \cdot 10^{-10}$	5.00	2	$6.55 \cdot 10^{-14}$	6.99	3		

Table 4.4: Angular Integral Test : $\gamma = \delta^2$

δ	m	abs error	order	m	abs error	order	m	abs error	order
0.1	1	$3.47 \cdot 10^{-5}$		2	$1.85 \cdot 10^{-7}$		3	$8.91 \cdot 10^{-10}$	
0.05	1	$1.31 \cdot 10^{-6}$	4.72	2	$2.22 \cdot 10^{-9}$	6.38	3	$4.08 \cdot 10^{-12}$	7.77
0.025	1	$4.30 \cdot 10^{-8}$	4.93	2	$1.92 \cdot 10^{-11}$	6.85	3	$9.68 \cdot 10^{-15}$	8.72
0.0125	1	$1.36 \cdot 10^{-9}$	4.98	2	$1.54 \cdot 10^{-13}$	6.96	3		

4.7.2 Radial Integral Only

In this section we test the procedure given in section 4.6.5 for estimating $I(\delta, \gamma)$ and verify equation (4.73). For a given $m \geq 0$ we expect to see a convergence rate of $O(\delta^{2m+3})$. We only test cases in which $\gamma = O(\delta^2)$. We use the locally flat cutoff function given by equation (A.1) with $\eta = 1/4$. For our test input functions we use

$$z(r) = a\sqrt{1-r^2} - a, \quad z_r(r) = \frac{-ar}{\sqrt{1-r^2}}, \quad f(r) = \sqrt{1 + z_r^2(r)}$$

Table 4.5: Angular Integral Test : $\gamma = -\delta^2$

δ	m	abs error	order	m	abs error	order	m	abs error	order
0.1	1	$1.74 \cdot 10^{-5}$		2	$4.49 \cdot 10^{-8}$		3	$1.67 \cdot 10^{-11}$	
0.05	1	$5.69 \cdot 10^{-7}$	4.93	2	$3.87 \cdot 10^{-10}$	6.86	3	$1.05 \cdot 10^{-13}$	7.31
0.025	1	$1.80 \cdot 10^{-8}$	4.98	2	$3.11 \cdot 10^{-12}$	6.96	3	$2.40 \cdot 10^{-16}$	8.77
0.0125	1	$5.66 \cdot 10^{-10}$	4.99	2	$2.45 \cdot 10^{-14}$	6.99	3		

Table 4.6: Angular Integral Test : $\gamma = \delta/6$

δ	m	abs error	order	m	abs error	order	m	abs error	order
0.1	1	$3.92 \cdot 10^{-5}$		2	$1.53 \cdot 10^{-7}$		3	$3.60 \cdot 10^{-10}$	
0.05	1	$2.51 \cdot 10^{-6}$	3.97	2	$2.91 \cdot 10^{-9}$	5.71	3	$3.16 \cdot 10^{-12}$	6.83
0.025	1	$1.58 \cdot 10^{-7}$	3.99	2	$4.86 \cdot 10^{-11}$	5.90	3	$1.57 \cdot 10^{-14}$	7.66
0.0125	1	$9.88 \cdot 10^{-9}$	4.00	2	$7.79 \cdot 10^{-13}$	5.96	3		

Table 4.7: Angular Integral Test : $\gamma = -\delta/4$

δ	m	abs error	order	m	abs error	order	m	abs error	order
0.1	1	$4.99 \cdot 10^{-5}$		2	$2.52 \cdot 10^{-7}$		3	$1.60 \cdot 10^{-9}$	
0.05	1	$2.97 \cdot 10^{-6}$	4.07	2	$3.47 \cdot 10^{-9}$	6.19	3	$4.57 \cdot 10^{-12}$	8.45
0.025	1	$1.78 \cdot 10^{-7}$	4.06	2	$4.76 \cdot 10^{-11}$	6.18	3	$1.27 \cdot 10^{-14}$	8.49
0.0125	1	$1.08 \cdot 10^{-8}$	4.04	2	$6.89 \cdot 10^{-13}$	6.11	3		

with parameter $a = 5$. This radial integral arises when computing a localized single layer potential with unit density on the oblate ellipsoid given by equation (4.74) with parameter $a = 5$. For the *exact* integral, we compute the radial integral to machine precision using the techniques in appendix C. Since we are testing the radial integration method by itself there is no angular error.

The results for the singular case ($\gamma = 0$) are shown in table 4.8. The results for

Table 4.8: Radial Integral Test : $\gamma = 0$

δ	m	abs error	order	m	abs error	order	m	abs error	order
0.1	1	$9.02 \cdot 10^{-5}$		2	$4.02 \cdot 10^{-6}$		3	$7.98 \cdot 10^{-7}$	
0.05	1	$2.99 \cdot 10^{-6}$	4.92	2	$3.67 \cdot 10^{-8}$	6.77	3	$1.81 \cdot 10^{-9}$	8.79
0.025	1	$9.48 \cdot 10^{-8}$	4.98	2	$2.99 \cdot 10^{-10}$	6.94	3	$3.67 \cdot 10^{-12}$	8.94
0.0125	1	$2.97 \cdot 10^{-9}$	4.99	2	$2.36 \cdot 10^{-12}$	6.99	3	$7.25 \cdot 10^{-15}$	8.99

the small distance nearly singular case where the point is first outside the surface

($\gamma = \delta^4$) and then inside the surface ($\gamma = -\delta^4$) are shown in tables 4.9 and 4.10. The results for the medium distance nearly singular case where the point is first

Table 4.9: Radial Integral Test : $\gamma = \delta^4$

δ	m	abs error	order	m	abs error	order	m	abs error	order
0.1	1	$9.02 \cdot 10^{-5}$		2	$4.01 \cdot 10^{-6}$		3	$7.96 \cdot 10^{-7}$	
0.05	1	$2.99 \cdot 10^{-6}$	4.92	2	$3.67 \cdot 10^{-8}$	6.77	3	$1.81 \cdot 10^{-9}$	8.78
0.025	1	$9.48 \cdot 10^{-8}$	4.98	2	$2.99 \cdot 10^{-10}$	6.94	3	$3.67 \cdot 10^{-12}$	8.94
0.0125	1	$2.97 \cdot 10^{-9}$	4.99	2	$2.36 \cdot 10^{-12}$	6.98	3	$7.25 \cdot 10^{-15}$	8.99

Table 4.10: Radial Integral Test : $\gamma = -\delta^4$

δ	m	abs error	order	m	abs error	order	m	abs error	order
0.1	1	$9.02 \cdot 10^{-5}$		2	$4.02 \cdot 10^{-6}$		3	$8.00 \cdot 10^{-7}$	
0.05	1	$2.98 \cdot 10^{-6}$	4.92	2	$3.67 \cdot 10^{-8}$	6.77	3	$1.81 \cdot 10^{-9}$	8.79
0.025	1	$9.48 \cdot 10^{-8}$	4.98	2	$2.99 \cdot 10^{-10}$	6.94	3	$3.67 \cdot 10^{-12}$	8.94
0.0125	1	$2.97 \cdot 10^{-9}$	4.99	2	$2.36 \cdot 10^{-12}$	6.99	3	$7.25 \cdot 10^{-15}$	8.99

outside the surface ($\gamma = \delta^2$) and then inside the surface ($\gamma = -\delta^2$) are shown in tables 4.11 and 4.12. In all test cases, we indeed see the expected convergence rate

Table 4.11: Radial Integral Test : $\gamma = \delta^2$

δ	m	abs error	order	m	abs error	order	m	abs error	order
0.1	1	$8.27 \cdot 10^{-5}$		2	$3.37 \cdot 10^{-6}$		3	$5.77 \cdot 10^{-7}$	
0.05	1	$3.19 \cdot 10^{-6}$	4.70	2	$3.50 \cdot 10^{-8}$	6.59	3	$1.66 \cdot 10^{-9}$	8.44
0.025	1	$1.06 \cdot 10^{-7}$	4.92	2	$2.95 \cdot 10^{-10}$	6.89	3	$3.60 \cdot 10^{-12}$	8.85
0.0125	1	$3.36 \cdot 10^{-9}$	4.98	2	$2.35 \cdot 10^{-12}$	6.97	3	$7.32 \cdot 10^{-15}$	8.94

of $O(\delta^{2m+3})$.

Table 4.12: Radial Integral Test : $\gamma = -\delta^2$

δ	m	abs error	order	m	abs error	order	m	abs error	order
0.1	1	$8.97 \cdot 10^{-5}$		2	$4.00 \cdot 10^{-6}$		3	$9.39 \cdot 10^{-7}$	
0.05	1	$2.68 \cdot 10^{-6}$	5.07	2	$3.71 \cdot 10^{-8}$	6.75	3	$1.89 \cdot 10^{-9}$	8.96
0.025	1	$8.30 \cdot 10^{-8}$	5.01	2	$3.00 \cdot 10^{-10}$	6.95	3	$3.72 \cdot 10^{-12}$	8.99
0.0125	1	$2.58 \cdot 10^{-9}$	5.01	2	$2.37 \cdot 10^{-12}$	6.99	3	$7.28 \cdot 10^{-15}$	8.98

4.7.3 Angular and Radial Integrals Combined

In this section, we execute a combined test of the angular integral method described in section 4.2.1 and the radial integral method described in section 4.2.2 to evaluate the localized single layer potential given by equation (4.2) with unit density, $\mu = 1$. For each of our three combined tests we have $\gamma = O(\delta^2)$. Thus, for a given m, the order of the angular method is $O(\delta^{2m+3})$ and the order of the radial method is $O(\delta^{2m+3})$. By the triangle inequality, the expected order of the combined method is also $O(\delta^{2m+3})$. Note that our combined approximation method uses $(2m+1)(2m)+1$ sample points. More specifically, there are $(2m+1)$ angular samples and for each angular sample we need $(2m+1)$ radial points but the middle radial point is the same for each angular sample. As usual, we use the locally flat cutoff function given by equation (A.1) with $\eta = 1/4$ and our test surface is the oblate ellipsoid given by equation (4.74) with parameter $a = 5$. For the *exact* integral we compute the radial integral to machine precision using the techniques in appendix C and use an angular quadrature spacing of $h^* = \pi/25$. We present data for $m \in \{1, 2, 3\}$ and verify that the observed order is indeed the predicted order of $O(\delta^{2m+3})$.

In tables 4.13, 4.14, and 4.15 we present the numerical data for the test cases corresponding to the singular case ($\gamma = 0$), the nearly singular case where the point outside the surface ($\gamma = \delta^2$), and the nearly singular case where the point is inside the surface ($\gamma = -\delta^2$).

Table 4.13: Combined Angular and Radial Test : $\gamma = 0$

δ	m	abs error	order	m	abs error	order	m	abs error	order
0.1	1	$8.73 \cdot 10^{-5}$		2	$4.29 \cdot 10^{-6}$		3	$6.51 \cdot 10^{-7}$	
0.05	1	$2.86 \cdot 10^{-6}$	4.93	2	$3.78 \cdot 10^{-8}$	6.83	3	$1.45 \cdot 10^{-9}$	8.81
0.025	1	$9.06 \cdot 10^{-8}$	4.98	2	$3.05 \cdot 10^{-10}$	6.95	3	$2.92 \cdot 10^{-12}$	8.95
0.0125	1	$2.84 \cdot 10^{-9}$	5.00	2	$2.40 \cdot 10^{-12}$	6.99	3	$5.76 \cdot 10^{-15}$	8.99

Table 4.14: Combined Angular and Radial Test : $\gamma = \delta^2$

δ	m	abs error	order	m	abs error	order	m	abs error	order
0.1	1	$1.12 \cdot 10^{-4}$		2	$3.40 \cdot 10^{-6}$		3	$4.73 \cdot 10^{-7}$	
0.05	1	$4.12 \cdot 10^{-6}$	4.76	2	$3.46 \cdot 10^{-8}$	6.62	3	$1.33 \cdot 10^{-9}$	8.47
0.025	1	$1.35 \cdot 10^{-7}$	4.93	2	$2.89 \cdot 10^{-10}$	6.90	3	$2.86 \cdot 10^{-12}$	8.86
0.0125	1	$4.27 \cdot 10^{-9}$	4.98	2	$2.30 \cdot 10^{-12}$	6.97	3	$6.08 \cdot 10^{-15}$	8.88

4.8 Numerical Results II : Complex Implicitly Defined Surfaces

In this section, we test our $O(1)$ local quadrature algorithm for computing the localized single layer potential given by equation (4.2) with unit density $\mu = 1$ on two complex implicitly defined surfaces. The testing methodology is similar to that discussed in section 4.7.3 except that the surfaces under test are implicitly defined. For the tests in this section, we fix $m = 3$ and only consider cases where $\gamma = O(\delta^2)$. Thus, the predicted order of convergence for each of the our numerical studies in this

Table 4.15: Combined Angular and Radial Test : $\gamma = -\delta^2$

δ	m	abs error	order	m	abs error	order	m	abs error	order
0.1	1	$4.45 \cdot 10^{-5}$		2	$4.72 \cdot 10^{-6}$		3	$7.69 \cdot 10^{-7}$	
0.05	1	$1.43 \cdot 10^{-6}$	4.96	2	$4.00 \cdot 10^{-8}$	6.88	3	$1.51 \cdot 10^{-9}$	8.99
0.025	1	$4.48 \cdot 10^{-8}$	4.99	2	$3.18 \cdot 10^{-10}$	6.97	3	$2.96 \cdot 10^{-12}$	9.00
0.0125	1	$1.40 \cdot 10^{-9}$	5.00	2	$2.50 \cdot 10^{-12}$	6.99	3	$6.15 \cdot 10^{-15}$	8.91

section is $O(\delta^9)$. As in section 4.7.3, for the *exact* integral we compute the radial integral to machine precision using the techniques in appendix C and use an angular quadrature spacing of $h^* = \pi/25$. One difference in the implicit case, however, is that we have to use the technique described in section 4.1.3 to sample the height function because we do not have an explicit formula.

Recall that each evaluation point x can be written as $x = x_n + x_p$ where x_p is called the *projected evaluation point* and is the point on the surface with the minimum distance to x. For our $O(1)$ local integration method, we use a polar grid of $(2m+1)(2m)+1$ points where x_p is at the center of the grid. Since we use $m = 3$, there are $(2m+1)(2m) = 42$ additional samples of the height function and its derivatives required. In all cases, we sample $F(s,t)$, the height function $Z(s,t)$, and the first derivatives $Z_s(s,t)$ and $Z_t(s,t)$ using the techniques described in section 4.1.3. Using the values of F, Z, Z_s, and Z_t at the grid points, we can compute the samples of f, z, and z_r needed to estimate the radial integrals as described in section 4.6.5. Note that the vectors u and v in the matrix $M = \{u, v, w\}$ mentioned in section 4.1.3 are only determined up to a rotation around w. To minimize symmetry, we always set u and v to be the principal directions rotated counterclockwise $\pi/7$ radians around $w = \nu(x_p)$.

As usual, we use the locally flat cutoff function given by equation (A.1) with $\eta = 1/4$.

4.8.1 Double Torus

In this section, our test surface $\mathcal{S}$ is the double torus whose level set function is given by equation (B.1). For our numerical tests, we use the three projected evaluation points $\{x_p^1, x_p^2, x_p^3\}$ whose coordinates are described in table 4.16. In addition, the principal curvatures, κ_1 and κ_2, are given for each projected evaluation point.

For the first test we put $\gamma = 0$. In this case, the i^{th} evaluation point is $x^i = x_p^i$.

Table 4.16: Projected Evaluation Points : Double Torus

i	$x_p^i \cdot e_1$	$x_p^i \cdot e_2$	$x_p^i \cdot e_3$	κ_1^i	κ_2^i
1	0.62501433494088	0.01	0.01	-6.00	3.81
2	0.89964275194013	0.01	0.01	-4.17	2.66
3	1.19254924926733	0.01	0.01	-0.81	-0.51

The results for all $i \in \{1, 2, 3\}$ are shown in table 4.17. Note that the errors are larger at the points with large curvature.

Table 4.17: Double Torus Local : $\gamma = 0$

δ	i	abs error	order	i	abs error	order	i	abs error	order
0.1	1	$5.52 \cdot 10^{-6}$		2	$1.36 \cdot 10^{-6}$		3	$3.72 \cdot 10^{-10}$	
0.05	1	$1.45 \cdot 10^{-8}$	8.57	2	$3.50 \cdot 10^{-9}$	8.60	3	$6.28 \cdot 10^{-13}$	9.21
0.025	1	$3.08 \cdot 10^{-11}$	8.88	2	$7.39 \cdot 10^{-12}$	8.89	3	$1.18 \cdot 10^{-15}$	9.06
0.0125	1	$6.14 \cdot 10^{-14}$	8.97	2	$1.47 \cdot 10^{-14}$	8.97	3		

In the next test we put $\gamma = \delta^2$. In this case, the i^{th} evaluation point is $x^i = x_p^i + \delta^2 \nu(x_p^i)$. The results for all $i \in \{1, 2, 3\}$ are shown in table 4.18.

Table 4.18: Double Torus Local : $\gamma = \delta^2$

δ	i	abs error	order	i	abs error	order	i	abs error	order
0.1	1	$4.26 \cdot 10^{-6}$		2	$1.20 \cdot 10^{-6}$		3	$5.41 \cdot 10^{-10}$	
0.05	1	$1.39 \cdot 10^{-8}$	8.26	2	$3.53 \cdot 10^{-9}$	8.41	3	$1.37 \cdot 10^{-12}$	8.62
0.025	1	$3.13 \cdot 10^{-11}$	8.80	2	$7.76 \cdot 10^{-12}$	8.83	3	$3.20 \cdot 10^{-15}$	8.74
0.0125	1	$6.32 \cdot 10^{-14}$	8.95	2	$1.55 \cdot 10^{-14}$	8.97	3		

4.8.2 Orthocircles

In this section, our test surface $\mathcal{S}$ is the orthocircles surface whose level set function is given by equation (B.2). For our numerical tests, we use the three projected eval-

uation points $\{x_p^1, x_p^2, x_p^3\}$ whose coordinates are described in table 4.19. In addition, the principal curvatures, κ_1 and κ_2, are given for each projected evaluation point.

Table 4.19: Projected Evaluation Points : Orthocircles

i	x_1^i	x_2^i	x_3^i	κ_1^i	κ_2^i
1	0.15741323309941	0.55	0.75	-3.80	1.70
2	0.19926311469040	0.6	0.75	-8.44	1.71
3	0.21749444292873	0.65	0.75	-19.5	1.47

For the first test we put $\gamma = 0$. In this case, the i^{th} evaluation point is $x^i = x_p^i$. The results for all $i \in \{1, 2, 3\}$ are shown in table 4.20. Note that as with the double torus example, the errors are larger at the points with large curvature.

Table 4.20: Orthocircles Local : $\gamma = 0$

δ	i	abs error	order	i	abs error	order	i	abs error	order
0.05	1	$3.62 \cdot 10^{-8}$		2	$1.13 \cdot 10^{-5}$		3	$1.06 \cdot 10^{-4}$	
0.025	1	$5.22 \cdot 10^{-11}$	9.44	2	$1.16 \cdot 10^{-8}$	9.92	3	$2.15 \cdot 10^{-7}$	8.95
0.0125	1	$9.49 \cdot 10^{-14}$	9.10	2	$1.93 \cdot 10^{-11}$	9.23	3	$4.31 \cdot 10^{-10}$	8.96
0.00625	1			2	$3.64 \cdot 10^{-14}$	9.06	3	$8.45 \cdot 10^{-13}$	8.99

In the next test we put $\gamma = -\delta^2$. In this case, the i^{th} evaluation point is $x^i = x_p^i - \delta^2 \nu(x_p^i)$. The results for all $i \in \{1, 2, 3\}$ are shown in table 4.21.

Table 4.21: Orthocircles Local : $\gamma = -\delta^2$

δ	i	abs error	order	i	abs error	order	i	abs error	order
0.05	1	$4.45 \cdot 10^{-8}$		2	$1.37 \cdot 10^{-5}$		3	$6.28 \cdot 10^{-5}$	
0.025	1	$6.41 \cdot 10^{-11}$	9.44	2	$1.26 \cdot 10^{-8}$	10.09	3	$2.32 \cdot 10^{-7}$	8.08
0.0125	1	$1.17 \cdot 10^{-13}$	9.09	2	$2.07 \cdot 10^{-11}$	9.25	3	$4.37 \cdot 10^{-10}$	9.05
0.00625	1			2	$3.86 \cdot 10^{-14}$	9.06	3	$8.44 \cdot 10^{-13}$	9.02

Appendix A

Locally Flat Cutoff Function Details

A standard tool in analysis is the C_c^∞ bump function $b(r) = e^{\frac{r^2}{r^2-1}}$ for $|r| < 1$ and $b(r) = 0$ otherwise. The graph is shown in figure A.1. For a parameter $\eta \in (0, 1)$,

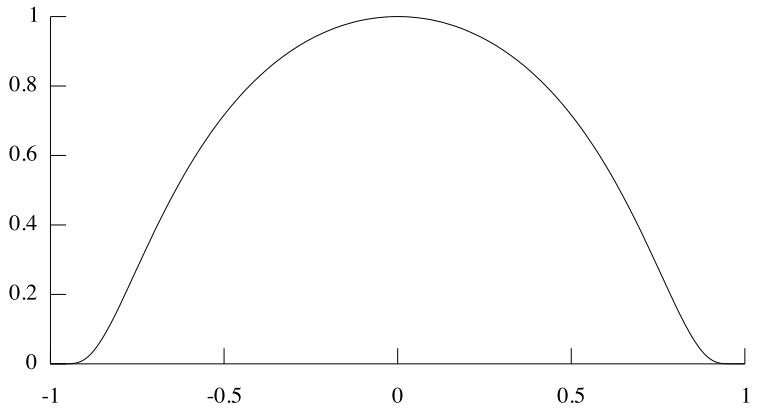

FIGURE A.1: Bump Function

we design a cutoff function that is equal to 1 on $[-\eta, \eta]$. For $|r| < 1$ define $\zeta^+(r) = \frac{b(r)}{b(r)+b(r-1-\eta)}$ and $\zeta^-(r) = \frac{b(r)}{b(r)+b(r+1+\eta)}$. These functions are 1 on $[-\eta, \eta]$ but not compactly supported. We thus define $\zeta(r) = \zeta^+(r)$ for $r \in [0, 1)$ and $\zeta(r) = \zeta^-(r)$ for $r \in (-1, 0]$. Using the fact that b is an even function, we dispense with the piecewise definition and use

$$\zeta(r) = \frac{b(r)}{b(r) + b(|r| - 1 - \eta)} \tag{A.1}$$

The graph for $\eta = 1/2$ is shown in figure A.2.

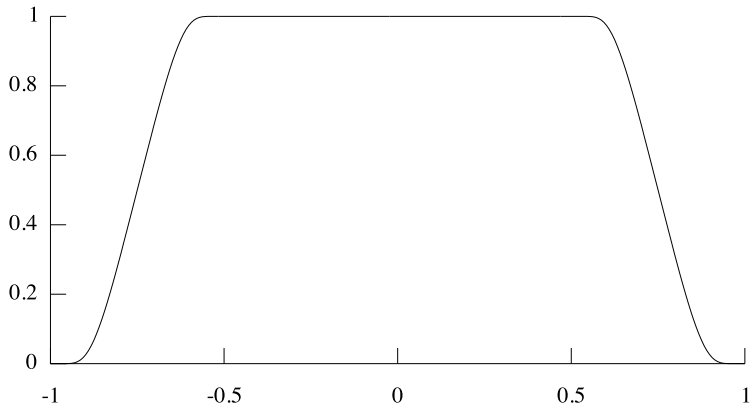

FIGURE A.2: Locally Flat Cutoff Function : $\eta = 1/2$

Appendix B

Three Complex Implicitly Defined Surfaces

For many of our numerical tests, we compute various integrals over the following three complex implicitly defined surfaces. The first two of these surfaces are used for integration testing in [8].

The first surface is the *double torus* which is given as the zero set of the function

$$\phi(x) = ((1.2 - x_1^2)x_1^2 - x_2^2)^2 + x_3^2 - 0.1 \tag{B.1}$$

A bounding box is specified by $b = (1.25, 1.25, 0.5)$. The double torus surface has genus two.

The second surface is the *orthocircles* which is given as the zero set of the function

$$\begin{aligned}\phi(x) = ((x_1^2 + x_2^2 - 1)^2 + x_3^2)((x_2^2 + x_3^2 - 1)^2 + x_1^2)((x_3^2 + x_1^2 - 1)^2 + x_2^2) \\ -a^2(1 + b(x_1^2 + x_2^2 + x_3^2))\end{aligned} \tag{B.2}$$

with parameters $a = 0.075$ and $b = 3$. A bounding box is specified by $b = (1.5, 1.5, 1.5)$. The orthocircles surface has genus seven.

The third surface is the *tanglecube* which is given as the zero set of the function

$$\phi(x) = x_1^4 - 5x_1^2 + x_2^4 - 5x_2^2 + x_3^4 - 5x_3^2 + 10 \tag{B.3}$$

A bounding box is specified by $b = (2.5, 2.5, 2.5)$. The tanglecube surface has genus five.

Appendix C

Computing Radial Integrals To Machine Precision

In this section we consider how to compute the radial integral given by equation (4.8) with an absolute error close to machine precision (we use 10^{-16} for our stopping criteria). We use these high precision radial integration methods for numerical tests where we need the *exact* value of a radial integral.

In the singular case, the integrand is a smooth function of r because

$$\frac{|r|f(r,\theta)}{(r^2+z^2(r,\theta))^{1/2}}\zeta_\delta((r^2+z^2(r,\theta))^{1/2}) = \frac{f(r,\theta)}{(1+z^2(r,\theta)/r^2)^{1/2}}\zeta_\delta(r(1+z^2(r,\theta)/r^2)^{1/2})$$

and $z^2(r,\theta)/r^2$ is a smooth function of r for a fixed θ. Thus, since the boundary is eliminated by the cutoff function, the trapezoid rule is very accurate and machine precision can be obtained by using several hundred quadrature points.

The nearly singular case is more difficult because although there is no boundary, the integrand is not smooth at 0 because of the $|r|$ term. Thus we split the integral

up as

$$\begin{aligned}\int_0^{\delta} \frac{rf(r,\theta)}{(r^2+(z-\gamma)^2)^{1/2}}\zeta_\delta((r^2+(z-\gamma)^2)^{1/2})dr \\ + \int_{-\delta}^{0} \frac{-rf(r,\theta)}{(r^2+(z-\gamma)^2)^{1/2}}\zeta_\delta((r^2+(z-\gamma)^2)^{1/2})dr\end{aligned} \tag{C.1}$$

and consider using the trapezoid rule on each integral separately. Although this deals with the smoothness issue, we have introduced a boundary at 0. Since the integrand evaluated at $r = 0$ is 0, the trapezoid rule sum is the same is in the singular case but now the convergence is only $O(h^2)$. Therefore we apply the first correction given by the Euler-Maclaurin formula to increase the order to $O(h^4)$. For a general integrand $g(r)$, the correction is given by $-(1/12)h^2(g'(b) - g'(a))$. In the first integral of equation (C.1), $g'(0) = f(0,\theta)/\gamma$ and $g'(\delta) = 0$. In the second integral, $g'(-\delta) = 0$ and $g'(0) = -f(0,\theta)/\gamma$. Thus the total correction to add to the trapezoid rule sum to increase the order to $O(h^4)$ is $(1/6)h^2(f(0,\theta)/\gamma)$. Although, this method does work well for relatively large gamma ($\gamma \geq \delta^2$), this is not a viable general purpose method for computing nearly singular integrals because although the convergence is fourth order in h, the constants blow up rapidly as $\gamma \to 0$.

To integrate nearly singular integrals with a very small γ such as $\gamma = \delta^4$ to high accuracy, we use the technique of *singularity subtraction*. Since these ideas are covered in more detail in section 4.4, we give only enough details to state the integral formula. For a fixed θ, we consider computing the radial integral

$$I = \int_{-\delta}^{\delta} \frac{|r|f(r,\theta)}{(r^2+(z(r,\theta)-\gamma)^2)^{1/2}}\zeta_\delta((r^2+(z(r,\theta)-\gamma)^2)^{1/2})dr$$

The technique is to add and subtract a nearly singular integral that can be computed exactly such that the order of the near singularity in the original integral is reduced.

In particular, we put

$$I = \int_{-\delta}^{\delta} \frac{|r|\left(f(r,\theta) - f(0,\theta)g(r,\theta)\right)}{(r^2 + (z(r,\theta)-\gamma)^2)^{1/2}} \zeta_\delta((r^2 + (z(r,\theta)-\gamma)^2)^{1/2})dr$$

$$+ \int_{-\delta}^{\delta} \frac{|r| f(0,\theta)g(r,\theta)}{(r^2 + (z(r,\theta)-\gamma)^2)^{1/2}} \zeta_\delta((r^2 + (z(r,\theta)-\gamma)^2)^{1/2})dr$$

where $g(r,\theta)$ is a helper function that is very near the identity that assists in integrating the last integral exactly. We define

$$y(r,\theta) = r\left(1 + \frac{z^2}{r^2} - \frac{2\gamma z}{r^2}\right)^{1/2} \tag{C.2}$$

and note that $y^2 = r^2 + z^2 - 2\gamma z$. Differentiating implicitly we see that

$$y_r(r,\theta) = \frac{r + z z_r - \gamma z_r}{y} \tag{C.3}$$

Next, we define $\alpha^2 = 1 - \gamma z_{rr}(0,\theta)$ and put

$$g(r,\theta) = \frac{y_r(r,\theta) y(r,\theta)}{\alpha^2 r} \tag{C.4}$$

and note that $g(r,\theta) = 1 + O(\gamma r) + O(r^2)$. Thus our choice of $g(r,\theta)$ satisfies the first requirement of being very close to the identity. Next we compute

$$I_0 = \int_{-\delta}^{\delta} \frac{|r| f(0,\theta)g(r,\theta)}{(r^2 + (z(r,\theta)-\gamma)^2)^{1/2}} \zeta_\delta((r^2 + (z(r,\theta)-\gamma)^2)^{1/2})dr$$

We first let $y^2 = r^2 + z^2 - 2\gamma z$ and use the definition of $g(r,\theta)$ to see that

$$I_0 = \frac{f(0,\theta)}{\alpha^2} \int_{-\delta}^{\delta} \frac{|y|}{(y^2+\gamma^2)^{1/2}} \zeta_\delta(y^2+\gamma^2)dy$$

Next we normalize by setting $u = y/\delta$ and $\beta = |\gamma|/\delta$ and see that

$$I_0 = \frac{f(0,\theta)\delta}{\alpha^2} \int_{-1}^{1} \frac{|u|}{(u^2+\beta^2)^{1/2}} \zeta(u^2+\beta^2)dy$$

Assuming that $\beta \leq \eta$ we get after using the substitution $v^2 = u^2 + \beta^2$ that

$$I_0 = \frac{f(0,\theta)\delta}{\alpha^2}(\zeta_0 - 2\beta)$$

where $\zeta_0 = \int_{-1}^{1} \zeta(u)du$. Thus we arrive at the following integral formula

$$I = \int_{-\delta}^{\delta} \frac{|r|\left(f(r,\theta) - f(0,\theta)g(r,\theta)\right)}{(r^2 + (z(r,\theta) - \gamma)^2)^{1/2}} \zeta_\delta((r^2 + (z(r,\theta) - \gamma)^2)^{1/2})dr + \frac{f(0,\theta)\delta}{\alpha^2}(\zeta_0 - 2\beta)$$

Because of the reduction in the order of the near singularity in the remaining integral, the trapezoid rule is very accurate for all γ. The theoretical justification of this fact is left for future work.

Appendix D

Centered Finite Difference Weights

Table D.1: Centered Finite Difference Weights : $m = 1$

$i\backslash l$	0	1	2
1	$-1/2$	0	$1/2$
2	1	-2	1

Table D.2: Centered Finite Difference Weights : $m = 2$

$i\backslash l$	0	1	2	3	4
1	$1/12$	$-2/3$	0	$2/3$	$-1/12$
2	$-1/12$	$4/3$	$-5/2$	$4/3$	$-1/12$
3	$-1/2$	1	0	-1	$1/2$
4	1	-4	6	-4	1

Table D.3: Centered Finite Difference Weights : $m = 3$

$i \backslash l$	0	1	2	3	4	5	6
1	$-1/60$	$3/20$	$-3/4$	0	$3/4$	$-3/20$	$1/60$
2	$1/90$	$-3/20$	$3/2$	$-49/18$	$3/2$	$-3/20$	$1/90$
3	$1/8$	-1	$13/8$	0	$-13/8$	1	$-1/8$
4	$-1/6$	2	$-13/2$	$28/3$	$-13/2$	2	$-1/6$
5	$-1/2$	2	$-5/2$	0	$5/2$	-2	$1/2$
6	1	-6	15	-20	15	-6	1

Bibliography

[1] J. T. Beale. A grid-based boundary integral method for elliptic problems in three dimensions. *SIAM J. Numer. Anal.*, 42(2):599–620, 2004.

[2] O. P. Bruno and L. A. Kunyansky. A fast, high-order algorithm for the solution of surface scattering problems: Basic implementation, tests, and applications. *Journal of Computational Physics*, 169(1):80–110, 2001.

[3] D. Dryanov and O. Kounchev. Multivariate Bernoulli functions and polyharmonically exact cubature formula of Euler-Maclaurin. *Math. Nachr.*, 226(1):65–83, 2001.

[4] G. Folland. *Introduction to Partial Differential Equations*. Princeton University Press, New Jersey, second edition, 1995.

[5] B. Fornberg. Generation of finite difference formulas on arbitrarily spaced grids. *Mathematics of Computation*, 51(184):699–706, 1988.

[6] J. Li. General explicit difference formulas for numerical differentiation. *Journal of Computational and Applied Mathematics*, 183(1):29–52, 2005.

[7] S. G. Mikhlin. *Mathematical Physics, an Advanced Course*. North-Holland Publishing Company, Amsterdam, 1970.

[8] C. Min and F. Gibou. Geometric integration over irregular domains with application to level-set methods. *Journal of Computational Physics*, 226(2):1432–1443, 2007.

[9] P. Smereka. The numerical approximation of a delta function with application to level set methods. *Journal of Computational Physics*, 211(1):77–90, 2006.

[10] L. Ying, G. Biros, and D. Zorin. A high-order 3D boundary integral equation solver for elliptic PDEs in smooth domains. *Journal of Computational Physics*, 219(1):247–275, 2006.

[11] L. Ying and D. Zorin. A simple manifold-based construction of surfaces of arbitrary smoothness. *ACM Transactions on Graphics (TOG)*, 23(3):271–275, 2004.

Biography

Jason Robert Wilson was born September 20, 1971 in Jasper, Indiana. In May of 1993 he earned a B.S. in computer science from Rose-Hulman Institute of Technology. In May of 1996 he obtained a M.S. in computer science from the University of North Carolina at Chapel Hill. While at UNC Chapel Hill, he was supported by a National Science Foundation Graduate Research Fellowship.

After a brief career as a software engineer, he returned to academic pursuits and in May of 2004 he earned a M.S. in mathematics from California State University at San Marcos. Finally, in September 2010 he earned a Ph.D. in mathematics from Duke University. Starting in the Fall 2010 semester, he will be an Instructor of Mathematics at Virginia Tech University.